



Glacier expansion on Baffin Island during early Holocene cold reversals

Sarah E. Crump^{a,*}, Nicolás E. Young^b, Gifford H. Miller^a, Simon L. Pendleton^{a,c}, Joseph P. Tulenko^d, Robert S. Anderson^a, Jason P. Briner^d

^a INSTAAR and Geological Sciences, University of Colorado Boulder, 4001 Discovery Drive, Boulder, CO, USA

^b Lamont-Doherty Earth Observatory, Columbia University, 61 Rte 9W, Palisades, NY, USA

^c Woods Hole Oceanographic Institution, 86 Water St., Woods Hole, MA, USA

^d Department of Geology, University at Buffalo, 126 Cooke Hall, Buffalo, NY, USA

ARTICLE INFO

Article history:

Received 12 February 2020

Received in revised form

6 June 2020

Accepted 8 June 2020

Available online xxx

Keywords:

Holocene

Paleoclimatology

Glaciology

Arctic

Cosmogenic isotopes

Glacial geomorphology

Abrupt climate change

ABSTRACT

The North Atlantic was a key locus for circulation-driven abrupt climate change in the past and could play a similar role in the future. Abrupt cold reversals, including the 8.2 ka event, punctuated the otherwise warm early Holocene in the North Atlantic region and serve as useful paleo examples of rapid climate change. In this work, we assess the cryospheric response to early Holocene climate history on Baffin Island, Arctic Canada, using cosmogenic radionuclide dating of moraines. We present 39 new ¹⁰Be ages from four sets of multi-crested early Holocene moraines deposited by cirque glaciers and ice cap outlet glaciers, as well as erratic boulders along adjacent fiords to constrain the timing of regional deglaciation. The age of one moraine is additionally constrained by *in situ* ¹⁴C measurements, which confirm ¹⁰Be inheritance in some samples. All four moraines were deposited between ~9.2 and 8.0 ka, and their average ages coincide with abrupt coolings at 9.3 and 8.2 ka that are recorded in Greenland ice cores. Freshwater delivery to the North Atlantic that reduced the flux of warm Atlantic water into Baffin Bay may explain brief intervals of glacier advance, although moraine formation cannot be definitively tied to centennial-scale cold reversals. We thus explore other possible contributing factors, including ice dynamics related to retreat of Laurentide Ice Sheet outlet glaciers. Using a numerical glacier model, we show that the debuitressing effect of trunk valley deglaciation may have contributed to these moraine-building events. These new age constraints and process insights highlight the complex behavior of the cryosphere during regional deglaciation and suggest that multiple abrupt cold reversals—as well as deglacial ice dynamics—likely played a role in early Holocene moraine formation on Baffin Island.

© 2020 Elsevier Ltd. All rights reserved.

1. Introduction

1.1. Abrupt climate change during the early Holocene

The climate system is capable of abrupt changes when a threshold is crossed that shifts the climate system into a different state (National Research Council, 2002). Because of the potential for abrupt change in the near future (e.g., Lenton, 2011)—and the heightened societal vulnerability to rapid rates of climate change—examples of abrupt climate change in the paleorecord are particularly important to understand (Alley et al., 2003; Broecker,

2000). The sudden reduction or shutdown of Atlantic Meridional Overturning Circulation (AMOC), which is responsible for the transport of low-latitude heat to the Arctic, is a known mechanism for abrupt climate change (Broecker, 1991; Clark et al., 2002; Sgubin et al., 2017). A sudden influx of freshwater in key downwelling sites (e.g., the Labrador Sea) can effectively slow or shut down AMOC, reducing latitudinal heat transport and thus promoting high-latitude cooling.

Ice core and marine sediment records have revealed that AMOC-driven abrupt climate changes were common, semi-regular features of the glacial climate mode (Dansgaard et al., 1993; Johnsen et al., 1992; Rahmstorf, 2003; Schulz, 2002), and that similar but lower-amplitude abrupt events also occurred during the Holocene (Bond, 1997). Early Holocene abrupt cooling events appear prominently in Greenland ice-core isotope records at 9.3 and 8.2 ka,

* Corresponding author.

E-mail address: sarah.crump@colorado.edu (S.E. Crump).

punctuating what was an otherwise relatively warm period (Alley et al., 1997; Kobashi et al., 2007; Rasmussen et al., 2007; Thomas et al., 2007). The effects of the <200-year-long 8.2 ka event were particularly pronounced and widespread, with abrupt cooling in central Greenland of ~ 3 to 10 °C and lesser cooling and drying throughout the Northern Hemisphere (Alley and Agustsdottir, 2005; Kobashi et al., 2007; Wanner et al., 2011). The 8.2 ka event is thought to have been caused by outburst floods of glacial lakes Agassiz and Ojibway that released massive amounts of freshwater through Hudson Strait, effectively shutting off deepwater formation in the Labrador Sea and causing a temporary reduction in AMOC with associated terrestrial cooling (Barber et al., 1999; Clarke et al., 2004; Jennings et al., 2015; Kleiven et al., 2008; LeGrande et al., 2006). Distinct detrital carbonate peaks in marine sediment from the Labrador Shelf indicate earlier freshwater pulses through Hudson Strait between ~ 11.5 and 9 ka, suggesting that multiple episodes of AMOC weakening may have resulted in brief regional cooling events during the early Holocene (Jennings et al., 2015).

Because small glaciers and ice caps respond sensitively to temperature changes, the moraine record from the North Atlantic region can help elucidate the occurrence and nature of abrupt climatic shifts during the early Holocene. Given the complex set of factors that can contribute to alpine glacier advance and moraine formation, however, a nuanced assessment of the spatiotemporal patterns of early Holocene moraines, as well as their possible causative factors, is warranted.

1.2. The early Holocene moraine record in the Baffin Bay region

Outlet glaciers of the Greenland and Laurentide ice sheets, as well as independent alpine glaciers and ice caps on eastern Baffin Island, Arctic Canada (Fig. 1), formed distinct sets of moraines during the early Holocene. In West Greenland, early Holocene

moraines spanning several hundred kilometers of the ice-free coastal area have been designated 'Fjord Stade moraines' and indicate multiple stages of early Holocene ice-margin stabilization (Donner and Jungner, 1975; Weidick, 1972, 1968). Extensive dating efforts employing cosmogenic ^{10}Be and radiocarbon dating of threshold lake records have correlated these moraines with known abrupt cooling events at 9.3 and 8.2 ka (Corbett et al., 2011; Young et al., 2020a, 2011, 2013a).

On eastern Baffin Island, a complex set of lateral and end moraines found inside the Laurentide Last Glacial Maximum (LGM) and Late Glacial ice margins are collectively termed 'Cockburn' moraines (Andrews and Ives, 1978; Briner et al., 2009; Margreth et al., 2017; Miller and Dyke, 1974). Radiocarbon dating of glaciomarine features (e.g., radiocarbon samples GSC-1638 and St-3816 from ice-proximal deltas in Fig. 1b) and morphostratigraphic correlation broadly constrained the Cockburn substage to ~ 9.5 – 8.0 ka, suggesting glacier readvance(s) or stabilization during this period of overall postglacial retreat (Andrews and Ives, 1978; Briner et al., 2007). Cosmogenic ^{10}Be dating in the Ayr Valley of northeastern Baffin Island tightly constrained an alpine glacier advance to 8.2 ± 0.2 ka, coeval with Laurentide outlet glacier stillstands or readvances in nearby fiord systems, suggesting that ice masses of different sizes in this region responded sensitively to the 8.2 ka event (Young et al., 2012). More recently, ^{10}Be dating at the King Harvest moraine complex (Fig. 1b) yielded three distinct periods of glacier stabilization—including both independent alpine glaciers and Laurentide outlet glaciers—at ~ 11.8 ka, 10.3 ka, and 9.2 ka (Young et al., 2020a). This new age control suggests that ice masses on Baffin Island expanded, or at least paused in their retreat, in response to not just the 9.3 and 8.2 ka events that are well-defined in the Greenland ice core and moraine records, but to numerous cold reversals throughout the early Holocene.

Here, we expand upon previous efforts to determine the timing

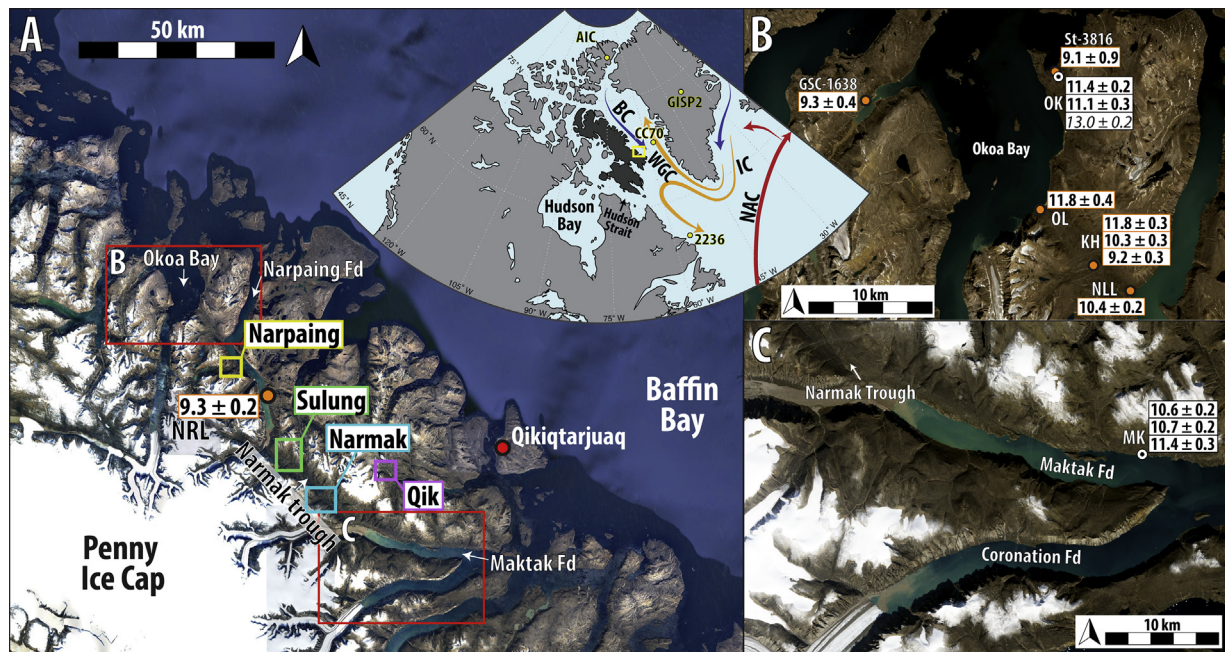


Fig. 1. Overview map of the study sites and LIS deglaciation ages. A) Google Earth image of northern Cumberland Peninsula study area (NRL = Narpaing Fiord right lateral from Young et al. (2020a)). Inset map includes approximations of major North Atlantic currents (NAC = North Atlantic Current, IC = Irminger Current, WGC = West Greenland Current, and BC = Baffin Current; colors correspond to relative temperature of each) and locations of regional comparison records mentioned in the text (AIC = Agassiz Ice Cap). B) Landsat 8 true color image (taken 7/23/2019) of Okoa Bay area (OK = Okoa Bay erratic samples from this study; OL = Okoa Lateral, KH = King Harvest Moraine, and NLL = Narpaing Fiord left lateral from Young et al. (2020a); GSC-1638 and St-3816 are radiocarbon ages on shells from raised deltas from Miller (1973) as recalibrated with ± 2 SD uncertainty in Briner et al. (2009)). C) Landsat 8 true color image (taken 8/19/2019) of Maktak Fiord area (MK = Maktak Fiord erratic samples from this study). (For interpretation of the references to color in this figure legend, the reader is referred to the Web version of this article.)

of early Holocene glacier advances/stillstands on Cumberland Peninsula, Baffin Island. Specifically, we 1) assess the synchronicity of moraine construction across a broader region; 2) compare the moraine record of cirque glaciers and ice cap outlet glaciers in contrasting settings; and 3) explore possible mechanisms (both climatic and non-climatic) that can explain the observed spatio-temporal trends in early Holocene ice patterns. We present 33 new ^{10}Be ages and three *in situ* ^{14}C ages from four independent early Holocene moraines, two formed by small cirque glaciers and two formed by larger ice-cap outlet glaciers, as well as six ^{10}Be ages on erratic boulders from adjacent fiords. We then evaluate the inferred moraine depositional ages in the context of the broader Baffin Bay moraine record and North Atlantic climate records to gain insight into the sensitivity of various ice masses to abrupt climate change. Finally, we employ a 1D numerical glacier model to explore the potential role of a mechanical adjustment of tributary glaciers in response to trunk valley deglaciation, which may have contributed to transient glacier re-advances during the early Holocene.

2. Regional setting

2.1. Geologic and climatological setting

Cumberland Peninsula, on the southeast corner of Baffin Island, is on the uplifted eastern rim of the Canadian Shield (Dyke et al., 1982) and is mantled by the 6000-km² Penny Ice Cap, a remnant of the LIS, as well as hundreds of independent ice caps and cirque glaciers (Fig. 1). The region falls in the Middle Arctic vegetation zone and is colder than other landmasses at comparable latitudes due to the cooling influence of the Baffin Current, which transports Arctic Ocean-sourced water along the Baffin Island coast (Paull et al., 2017; Tang et al., 2004). At the nearest meteorological station in Qikiqtarjuaq, Nunavut (Fig. 1), the mean annual temperature is $-11.8\text{ }^{\circ}\text{C}$, and an average of 262 mm of precipitation (85% as snow) falls per year (1971–2000 Canadian Climate Normals, Environment Canada: <http://climate.weather.gc.ca>). Recent summer warming has led to negative mass balances for the glaciers and ice caps of Cumberland Peninsula, with mass losses increasing dramatically in the 21st century (Gardner et al., 2011, 2012; Miller et al., 2013).

While the extent of LGM ice in this area was once greatly debated (Miller and Dyke, 1974), marine and lake sediment data and cosmogenic radionuclide dating of glacial features demonstrate that predominantly cold-based ice covered nearly all of southern Baffin Island during peak glacial times, except for some of the high peaks near the coast (Margreth et al., 2016; Pendleton et al., 2019), and fast-moving ice flowed through the fiords to the continental shelf (Miller et al., 2002). The LIS retreated during the latest Pleistocene, with some evidence for stillstands and/or readvances on Cumberland Peninsula during Heinrich event 1 and the Younger Dryas (Corbett et al., 2016a; Margreth et al., 2017), although large chronological uncertainties make these links tentative. Many of the fiord systems of Baffin Island experienced rapid retreat between ~ 12 and 10 ka (Briner et al., 2009).

2.2. Fiord sample sites

To gain additional constraints on the timing of regional deglaciation, we sampled erratic boulders perched on bedrock flanking Okoa Bay and Maktak Fiord (Fig. 1). These fiords contained LIS outlet glaciers during full glacial conditions, and erratic boulders perched on bedrock serve as targets for estimating the timing of deglaciation. LIS outlet glaciers would have retreated past these points before cirque and ice cap outlet glaciers could have readvanced to form the independent moraine systems described below. Fiord sample exposure ages thus provide maximum ages that help

constrain early Holocene moraine formation timing. Radiocarbon ages from raised ice-proximal deltas in outer Okoa Bay calibrate to $\sim 9\text{ ka}$ (Fig. 1a) (Briner et al., 2009; Miller, 1973), providing a first estimate on the timing of deglaciation in the region. Both fiords currently receive meltwater from outlet glaciers of the Penny Ice Cap. Okoa Bay has a tidewater glacier at its head, whereas a $\sim 14\text{-km}$ -long sandur separates an outlet glacier of the Penny Ice Cap from the head of Maktak Fiord.

2.3. Early Holocene moraine systems

We targeted moraines in four valleys on the east coast of Cumberland Peninsula (Fig. 1) that we hypothesized were early Holocene (Cockburn) glacial features based on their positions (i.e., the first set of moraines downvalley from historical/Neoglacial moraines), morphology, and surface character. Specifically, the moraines are morphologically subdued and contain boulders with mature lichen cover and rest downvalley of the presumed late Holocene maximum extent of each glacier. Each was formed by local ice, rather than the Laurentide Ice Sheet, and is well within the LGM limit. The targeted moraines were deposited by tributary glaciers after substantial deglaciation of fiords and major through-valleys during what were presumably stillstands or minor readvances in the otherwise warm early Holocene. Characteristics of the four sites are summarized in Table 1 and described below.

Narpaing Valley (informal name) is an east-west oriented valley draining into Narpaing Fiord. Several tributary glaciers emanating from the plateau to the south fed into the main trunk valley and deposited arcuate end moraines on the valley floor following its deglaciation. We focused on the easternmost moraine complex, Narpaing Moraine, a double-crested end moraine formed by a cirque glacier with a northeast to northwest aspect (Fig. 2). The outer and inner crests of Narpaing Moraine are separated by a fluvial channel, and an exposure of lacustrine sediments to the west suggests that the glacier and/or moraines once dammed a lake on the valley floor. The extant cirque glacier terminus is currently $\sim 3.9\text{ km}$ upvalley of the inner moraine.

Sulung Valley is a small south-facing valley formed by a cirque glacier feeding into a prominent through-valley (informally called Narmak Trough) that connects Narpaing and Maktak fiords (Fig. 2). Sulung Valley neither holds an extant glacier, presumably due to its south-facing aspect, nor displays any evidence of Neoglacial ice growth. We targeted a triple-crested end moraine (Sulung Moraine) that is situated 700 m asl and $\sim 500\text{ m}$ above the trough floor. Sulung Moraine cross-cuts a lateral moraine formed by ice flowing through the trough. Previous work by Dugdale (1972), including mapping and relative dating via weathering indices, concluded that the three crests formed in distinct advances at 35 ka , 23 ka , and 12.5 ka . However, subsequent work on the full-glacial extent of the LIS on southern Baffin Island (Miller et al., 2002) implied that the three nested moraines most likely were all deposited after the LGM.

Narmak Trough hosts a set of moraines that were formed by an outlet glacier from a northeast-facing ice cap (Fig. 2). The double-crested Narmak Moraine system formed after deglaciation of the Narmak Trough. The current ice cap outlet margin is $\sim 8\text{ km}$ from the inner moraine.

Qik Valley (informal name) is an extension of Kagittullu Fiord near the island of Qikiqtarjuaq. Two outlet glaciers fed by a small ice cap coalesce in the valley and formed a now-subdued end moraine positioned between lakes (Fig. 2). Clear trimlines define the glaciers' expanded state during the late Holocene maximum, only 0.5 km from the early Holocene moraine. The two outlet glaciers have experienced net retreat of ~ 1.9 and 3.6 km from the late Holocene moraine.

Table 1
Early Holocene moraine characteristics.

Moraine	Latitude & Longitude	Elevation (m asl)	Paleo-glacier toe aspect	Type of ice mass	Catchment area (km ²)	Distance from extant glacier margin/cirque headwall (km)
Narpaing Moraine	67.727399°, −65.589690°	134	NW	Cirque	15.2	3.6/6.7
Sulung Moraine	67.523907°, −65.234423°	700	S	Cirque	9.2	NA/4.6
Narmak Moraine	67.444836°, −65.064955°	541	NE	Ice cap outlet	60.4	8.0/NA
Qik Moraine	67.504153°, −64.691601°	633	ENE	Ice cap outlet	55.4	1.9, 3.6/NA

3. Materials and methods

3.1. Field methods

We collected rock samples from the four moraines and fiord margins during the summers of 2014 and 2015. Using high-

resolution satellite imagery (WorldView, Digital Globe) and field observations, we mapped the areal extent of each moraine crest. We identified the most suitable boulders for sampling based on well-established criteria (e.g., Putkonen and Swanson, 2003) to minimize the possibility of shielding and previous exhumation or destabilization, which can compromise the ¹⁰Be exposure clock:

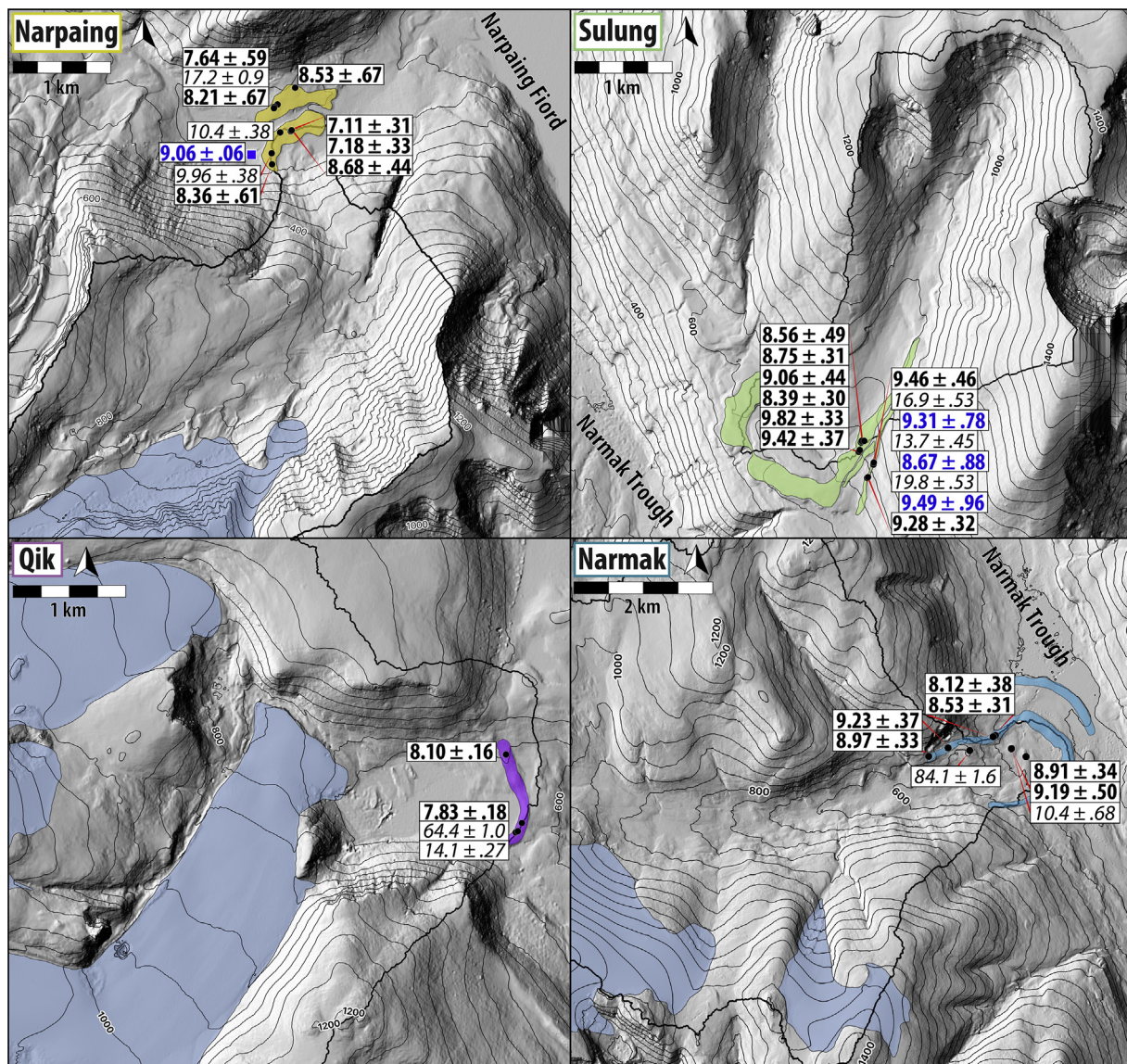


Fig. 2. Early Holocene moraines and exposure ages (ka) on hillshade renderings of 2-m DEMs (Arctic DEM) with elevation contours (in m) for each glacial valley. Light blue shading outlines modern ice extent, heavy black line denotes catchment area, and colored shading highlights approximate moraine area. ¹⁰Be ages with internal uncertainty are in black bolded text, with discarded outliers in italics. Radiocarbon date from a plant macrofossil in lacustrine sediment outboard of Narpaing moraine is denoted by blue square. *In situ* ¹⁴C ages from the Sulung outer moraine are in blue bolded text below their corresponding ¹⁰Be ages. (For interpretation of the references to color in this figure legend, the reader is referred to the Web version of this article.)

large size (>1 m high and 1 m³), stable position on or near the moraine crest, and substantial quartz content. We sampled horizontal or subhorizontal surfaces in the middle of the boulder wherever possible and noted cases of surface inclination as needed for adjusting production rate. In some cases, we also targeted boulders perched on bedrock inside of the moraine, which are largely immune to post-depositional shifting and should provide close minimum limiting ages for the moraine. In the case of Okoa Bay and Maktak Fiord, we exclusively targeted erratic boulders perched on bedrock. At Okoa, we sampled erratic boulders perched 38 m asl near the fiord mouth; samples locations are within 20 m of each other, so all ages should reflect the same exposure timing. At Maktak, we sampled erratic boulders perched 35–64 m asl along the middle of the fiord; sample locations span ~150 m laterally and should reflect roughly the same exposure timing. We sampled the uppermost (<4 cm) portion of selected boulders using a combination of a battery-powered angle grinder with diamond tip blade and hammer and chisel (Fig. 3). We recorded the location and elevation of each sample using a Garmin eTrex handheld GPS unit and measured topographic shielding using an inclinometer and compass azimuth in at least one location for each moraine crest.

3.2. Cosmogenic radionuclide extraction and analysis

3.2.1. ¹⁰Be samples

Mineral separation and ¹⁰Be extraction took place at the University of Colorado Cosmogenic Isotope Laboratory ($n = 33$; moraine boulders) and the University at Buffalo Glacier History Laboratory ($n = 6$; Okoa and Maktak fiord samples) using slightly modified versions of well-established protocols (Corbett et al., 2016a; Kohl and Nishiizumi, 1992; Schaefer et al., 2009; von Blanckenburg et al., 1996). Raw rock samples were crushed, milled, and sieved to separate the 250–500 μm fraction. Crushed samples were processed to separate pure quartz using standard techniques: dilute HCl and HF–HNO₃ acid etching to remove any organics and non-quartz minerals; froth flotation followed by heavy liquid separation for select samples to remove feldspars and mafic minerals; and final etching in dilute HF–HNO₃ acid. Quartz purity was determined by ICP-OES at the Laboratory of Environmental and Geological Studies at the University of Colorado Boulder.

We processed an aliquot of ~20–40 g of pure quartz spiked with ⁹Be carrier and then dissolved the samples in an HF–HNO₃ acid mixture (Table 2). One process blank (⁹Be carrier only) was prepared with each batch of 11 samples, following identical chemical treatments. Samples were converted to sulfides and then chlorides using H₂SO₄ and HCl, respectively. Fe and Ti were removed through high pH precipitation, followed by precipitation of Be and Al at pH 8. Be was separated from Al and other remaining ions via cation column chromatography. Be(OH)₂ was precipitated at pH 8, dried and combusted to form BeO, and then mixed with Niobium powder and packed into steel cylinders. ¹⁰Be/⁹Be isotope ratio measurements were made via accelerator mass spectrometry at the Purdue Rare Isotope Measurement (PRIME) Lab ($n = 33$; moraine boulders) and the Lawrence Livermore National Laboratory – Center for Accelerator Mass Spectrometry ($n = 6$; Okoa and Maktak samples). All samples are normalized to the 07KNSTD3110 standard that has a reported ratio of 2.85×10^{-12} (Nishiizumi et al., 2007).

3.2.2. *In situ* ¹⁴C samples

We selected three samples from the Sulung outer moraine that have what we interpret to be anomalously old ¹⁰Be ages for *in situ* ¹⁴C dating (Table 3). Long-lived nuclides such as ¹⁰Be ($t_{1/2} = \sim 1.4$ Ma) must be removed from the landscape via sufficient subglacial erosion, but *in situ* ¹⁴C is unique because its relatively



Fig. 3. Representative sample boulders from moraine crests at Nairpaing (A) and Narmak (B) moraines. Reported ¹⁰Be ages (ka) include internal uncertainty.

short half-life ($t_{1/2} = 5700$ years; National Nuclear Data Center, B.N.L., www.nndc.bnl.gov) allows for previously accumulated *in situ* ¹⁴C to decay away to undetectable levels after ~25–30 ka of burial of a surface. Thus, *in situ* ¹⁴C measurements are attractive in environments characterized by minimally erosive ice that is not everywhere capable of resetting the cosmogenic clock between periods of exposure. When paired with ¹⁰Be concentrations suspected to be influenced by isotopic inheritance, *in situ* ¹⁴C measurements can simultaneously quantify the timing of the last deglaciation and the amount of inheritance in the paired ¹⁰Be inventories (e.g., Young et al., 2018).

Mineral separation for *in situ* ¹⁴C measurements was as described in section 3.2.1; aliquots from the same fraction of clean quartz were used for both ¹⁰Be and *in situ* ¹⁴C extraction. *In situ* ¹⁴C extraction was completed at the Lamont-Doherty Earth Observatory Cosmogenic Nuclide Laboratory following procedures described in Lamp et al. (2019), and final ¹⁴C measurements were completed at the Lawrence Livermore National Laboratory – Center for Accelerator Mass Spectrometry. Measured ¹⁴C concentrations are blank-corrected using a long-term laboratory blank value (Table 3). We note that the quartz aliquots underwent froth flotation to remove feldspars and micas, but the use of laurylamine, an organic compound, in this procedure can potentially contaminate *in situ* ¹⁴C measurements if quartz is not sufficiently etched following froth flotation (Nichols and Goehring, 2019). To ensure

Table 2
¹⁰Be data.

Feature	Sample ID	Latitude	Longitude	Elevation (masl)	Thickness (cm)	Density (g/cm ³)	Shielding correction	Quartz (g)	Be carrier added (g) ^a	¹⁰ Be/ ⁹ Be	Blank used for correction ^b	¹⁰ Be concentration (atoms/g)	¹⁰ Be uncertainty (atoms/g)	¹⁰ Be age (Lm) ^c	¹⁰ Be age internal uncertainty
Sulung outer	15BBS-01	67.524712	-65.230293	709	2.5	2.44	0.994	30.6326	0.5916	3.133E-13	A	1.437 E+05	4.436 E+03	16,924	525
	15BBS-03	67.523281	-65.230379	687	2.0	2.58	0.994	29.7406	0.5942	2.438E-13	A	1.144 E+05	3.708 E+03	13,705	446
	15BBS-05	67.523181	-65.230509	682	2.4	2.65	0.994	29.8449	0.5933	3.461E-13	A	1.640 E+05	4.378 E+03	19,843	532
	15BBS-02	67.524527	-65.230200	706	2.2	2.61	0.994	30.2144	0.5947	1.675E-13	C	8.032 E+04	3.875 E+03	9459	457
	15BBS-06	67.523187	-65.230529	687	2.1	2.58	0.994	30.0055	0.5952	1.604E-13	C	7.749 E+04	2.677 E+03	9280	321
	15BBS-14	67.526259	-65.234197	710	1.5	2.55	0.993	30.2620	0.5931	1.635E-13	A	7.334 E+04	4.162 E+03	8560	487
Sulung inner	15BBS-15	67.526187	-65.234767	710	2.4	2.50	0.993	30.0837	0.5933	1.649E-13	A	7.450 E+04	2.629 E+03	8754	310
	15BBS-19	67.525344	-65.234455	698	2.0	2.74	0.993	29.9369	0.5903	1.819E-13	A	8.274 E+04	2.811 E+03	9820	334
	15BBS-20	67.525162	-65.234547	696	1.7	2.51	0.993	30.0283	0.5906	1.757E-13	A	7.951 E+04	3.072 E+03	9418	365
	15BBS-16	67.526130	-65.234655	710	1.5	2.69	0.993	30.3429	0.5961	1.634E-13	D	7.760 E+04	3.794 E+03	9064	444
	15BBS-17	67.526023	-65.234773	706	2.4	2.58	0.993	24.7117	0.5950	1.218E-13	C	7.108 E+04	2.499 E+03	8388	296
	15BBS-04	67.440336	-65.081133	606	1.7	2.55	0.964	30.0058	0.5948	1.413E-13	B	6.752 E+04	2.469 E+03	8972	329
Narmak	15BNK-05	67.438459	-65.086233	663	1.8	2.54	0.978	30.0528	0.5962	1.551E-13	B	7.433 E+04	2.929 E+03	9229	365
	15BNK-06	67.443648	-65.068267	522	1.8	2.54	0.995	30.3316	0.5992	1.225E-13	B	5.811 E+04	2.693 E+03	8122	377
	15BNK-07	67.443980	-65.067680	515	1.8	2.54	0.995	30.2481	0.5952	1.281E-13	B	6.060 E+04	2.176 E+03	8529	307
	15BNK-12	67.442710	-65.055670	479	2.4	2.49	0.997	27.5832	0.6004	1.167E-13	B	6.095 E+04	2.290 E+03	8909	335
	15BNK-01	67.440970	-65.074030	573	1.9	2.65	0.988	30.0024	0.5948	1.259E-12	C	6.154 E+05	1.168 E+04	84,119	1631
	15BNK-10	67.443040	-65.061220	487	2.0	2.59	0.997	30.6235	0.4853	1.873E-13	D	7.182 E+04	4.686 E+03	10,394	680
	15BNK-11	67.442930	-65.061290	487	1.6	2.53	0.997	30.7715	0.4865	1.671E-13	D	6.376 E+04	3.473 E+03	9192	502
	15BNP-02	67.725978	-65.590101	138	2.2	2.77	0.985	30.0877	0.5989	9.940E-14	B	4.720 E+04	1.790 E+03	9958	379
	15BNP-01	67.725031	-65.589063	147	1.7	2.47	0.985	21.2325	0.5976	6.013E-14	C	4.027 E+04	2.921 E+03	8360	608
	15BNP-03	67.728061	-65.589955	129	1.7	2.62	0.985	30.0542	0.5953	1.027E-13	C	4.916 E+04	1.807 E+03	10,425	384
	15BNP-04	67.728620	-65.587514	129	2.9	2.55	0.985	30.2445	0.5957	7.059E-14	C	3.327 E+04	1.454 E+03	7113	311
Narpaing inner	15BNP-05	67.728558	-65.587545	131	2.4	2.71	0.985	30.5646	0.5972	8.668E-14	C	4.076 E+04	2.083 E+03	8675	444
	15BNP-06	67.728505	-65.587632	126	1.9	2.36	0.985	30.6304	0.5948	7.259E-14	C	3.375 E+04	1.548 E+03	7176	330
	15BNP-08	67.729958	-65.593449	128	2.5	2.61	0.976	26.3530	0.4910	8.658E-14	D	3.812 E+04	3.117 E+03	8213	673
	15BNP-09	67.730089	-65.593500	132	2.5	2.69	0.976	31.1504	0.4904	2.098E-13	D	8.012 E+04	3.949 E+03	17,235	853
	15BNP-10	67.730398	-65.592952	135	2.9	2.57	0.976	30.0703	0.4912	9.214E-14	D	3.566 E+04	2.748 E+03	7644	590
	15BNP-11	67.732426	-65.590364	143	2.3	2.64	0.976	17.0947	0.4853	6.124E-14	D	4.029 E+04	3.177 E+03	8526	674
Qik	2-M14-B128	67.506388	-64.697848	648	4.0	2.65	0.994	37.0761	0.2162	4.564E-13	E	6.418 E+04	1.266 E+03	8098	160
	2-M14-B129	67.501747	-64.690049	632	4.0	2.65	0.994	40.0051	0.2188	4.632E-13	E	6.114 E+04	1.399 E+03	7832	180
	2-M14-B130	67.501032	-64.690259	632	2.0	2.65	0.994	40.0416	0.2170	3.759E-12	E	5.035 E+05	7.662 E+03	64,357	995
	2-M14-B131	67.500886	-64.690609	619	2.0	2.65	0.994	40.0189	0.2167	8.313E-13	E	1.100 E+05	2.133 E+03	14,059	274
Okoa Fiord	15BOK-01	67.95261	-65.74335	38	3	2.65	0.981	35.9248	0.6060	1.132E-13	F	4.754 E+04	1.036 E+03	11,350	248
	15BOK-02	67.95267	-65.74307	38	2	2.65	0.981	24.0253	0.6044	7.482E-14	F	4.685 E+04	1.053 E+03	11,095	250
	15BOK-03	67.95274	-65.74319	38	2	2.65	0.981	24.4209	0.6044	8.885E-14	F	5.474 E+04	1.002 E+03	12,969	238
Maktak Fiord	15BMK-01	67.32599	-64.28902	64	2	2.65	0.986	40.3734	0.6041	1.249E-13	F	4.654 E+04	8.486 E+02	10,625	194
	15BMK-02	67.32607	-64.2896	62	3	2.65	0.986	27.7870	0.6040	8.583E-14	F	4.644 E+04	7.811 E+02	10,713	181
	15BMK-03	67.32571	-64.28609	35	2	2.65	0.986	37.0332	0.6071	1.181E-13	F	4.821 E+04	1.200 E+03	11,385	284

^a Carrier concentration is 369.5 ppm ($n = 33$; moraine boulders) or 372.5 ppm ($n = 6$; Okoa and Maktak fiord samples).

^b Blank values are as follows.

A: ¹⁰Be atoms were background-corrected using the process blank value of 1.75×10^5 atoms (¹⁰Be/⁹Be ratio of 1.19×10^{-14})

B: ¹⁰Be atoms were background-corrected using the process blank value of 4.95×10^4 atoms (¹⁰Be/⁹Be ratio of 3.38×10^{-15})

C: ¹⁰Be atoms were background-corrected using the process blank value of 3.22×10^4 atoms (¹⁰Be/⁹Be ratio of 2.19×10^{-15})

D: ¹⁰Be atoms were background-corrected using the process blank value of 4.51×10^4 atoms (¹⁰Be/⁹Be ratio of 3.68×10^{-15})

E: ¹⁰Be atoms were background-corrected using the process blank value of 6.71×10^4 atoms (¹⁰Be/⁹Be ratio of 1.25×10^{-14})

F: ¹⁰Be atoms were background corrected using the process blank value of 5.38×10^4 atoms (¹⁰Be/⁹Be ratio of 3.56×10^{-15})

^c Italicized ages are outliers excluded from summary statistics.

Table 3
In situ ¹⁴C extraction details.

Identification	Sample type	Date extracted	Quartz (g)	LLNL-CAMS #	Carbon yield (μg C)	Diluted carbon mass (μg C)	F _m measured	¹⁴ C/C _{total} (10 ⁻¹⁵)	¹⁴ C concentration (atoms g ⁻¹) ^a	¹⁴ C age – Lm (ka)	¹⁴ C age – LSDn (ka)
BLANK_3_5_19	process blank	3/5/19	NA	181,712	6.33 ± 0.07	726.9 ± 8.3	0.0041 ± 0.0001	1.84 ± 0.36	67,117 ± 13,007	NA	NA
15BSS-01	geologic	3/14/19	5.4312	181,709	9.56 ± 0.11	719.9 ± 8.2	0.0273 ± 0.0002	28.91 ± 0.40	170,624 ± 7691	9.31 ± 0.78	9.43 ± 0.79
15BSS-03	geologic	3/27/19	4.4803	181,940	23.19 ± 0.27	754.0 ± 8.6	0.0215 ± 0.0002	22.21 ± 0.40	161,288 ± 9239	8.67 ± 0.88	8.77 ± 0.89
15BSS-05	geologic	3/29/19	4.5748	181,941	11.74 ± 0.13	760.1 ± 8.7	0.0224 ± 0.0002	23.27 ± 0.40	168,284 ± 9084	9.49 ± 0.96	9.61 ± 0.98
BLANK_5_1_19	process blank	5/1/19	NA	181,942	6.60 ± 0.08	750.1 ± 8.6	0.0046 ± 0.0001	2.47 ± 0.35	92,935 ± 13,352	NA	NA
CRONUSA_5_3_19	standard	5/13/19	3.8111	181,939	51.08 ± 0.59	764.9 ± 8.8	0.0629 ± 0.0003	70.50 ± 0.39	679,521 ± 13,241	NA	NA

^a ¹⁴C concentrations for samples 15BSS-01, 15BSS-03, and 15BSS-05 are blank-corrected using a LDEO long-term value of 116.89 ± 37.31 × 10³ ¹⁴C atoms (n=27); this value includes BLANK_3_5_19. The ¹⁴C concentration for CRONUSA_5_3_19 is blank-corrected using a LDEO long-term value of 116.07 ± 36.89 × 10³ ¹⁴C atoms (n=28); this updated long-term value includes BLANK_5_1_19. Including the CRONUSA_5_3_19 measurement, the LDEO long-term CRONUS-A ¹⁴C concentration is 698.10 ± 25.38 × 10³ ¹⁴C atoms (n = 13).

the removal of any remnant laurylamine prior to *in situ* ¹⁴C extraction, quartz aliquots underwent a 24-hr shaker table bath in ~10% HNO₃ solution followed by a 90 min heated bath in 50% HNO₃ solution.

3.2.3. ¹⁰Be and *in situ* ¹⁴C age calculations

¹⁰Be and *in situ* ¹⁴C surface exposure ages were calculated using the regionally calibrated Baffin Bay ¹⁰Be and western Greenland *in situ* ¹⁴C production rate calibration datasets (Young et al., 2013b, 2014) and ‘Lm’ scaling as the effects in changes in the geomagnetic field are minimal at this high latitude (Lal, 1991; Stone, 2000). The Baffin Bay ¹⁰Be production rate calibration dataset consists of three independent calibration datasets, and one of these calibration sites serves as a dual ¹⁰Be–¹⁴C calibration dataset (Young et al., 2014). Ages are calculated using version 3 of the exposure age calculator found at <https://hess.ess.washington.edu/>, which implements an updated treatment of muon-based nuclide production (Balco, 2017; Balco et al., 2008). Topographic shielding corrections were determined using the CRONUS Earth web calculator (Marrero et al., 2016). We do not correct nuclide concentrations for snow cover or surface erosion; all samples are from windswept locations and many surfaces still retained primary glacial features. In addition, we make no correction for the effects of isostatic rebound because samples have experienced a similar uplift history over a similar timeframe as those used to calibrate the Baffin Bay production rate, and we use the reference production rate that does not include a correction for isostatic rebound (Young et al., 2020b). Individual ¹⁰Be ages are discussed with 1-sigma analytical uncertainties, and moraine ages exclude the ¹⁰Be production-rate uncertainty when we are comparing different moraine ages within our field area.

3.3. Statistical treatment of ¹⁰Be ages

Because the accuracy of ¹⁰Be as an exposure dating tool can be compromised by inherited radionuclide inventories, which produce too-old ages, and post-depositional destabilization and shielding, which produce too-young ages, it is critical to evaluate sets of ¹⁰Be ages for outliers before calculating feature means for further interpretation (Crump et al., 2017). While a variety of criteria have been used in previous studies (Balco, 2011), including both statistical tests for identifying outliers (e.g., Chauvenet’s criterion; Rinterknecht et al., 2006) and geomorphic justifications for preferring one extreme end of a distribution of ages (e.g., using the oldest age in a distribution; Putkonen and Swanson, 2003), we combine statistical and field observation-based approaches to robustly determine the central tendency of the dataset for each feature. To determine which outliers to exclude from further

analysis, we assessed sets of ages using three approaches:

- 1) We first plot the normal kernel density estimate of each feature, which incorporates the analytical (internal) uncertainty of each age as a gaussian distribution of possible “true” ages (Lowell, 1995). The normal kernel density estimate reveals the most likely depositional age of the moraine, if tightly clustered individual ages produce a distinct peak. Visual inspection of this plot allows exclusion of obvious outliers (e.g., Chen et al., 2015; Rood et al., 2011).
- 2) In some cases, secure ages from adjacent moraine crests or boulders on bedrock within the moraine help determine outliers based on morphostratigraphic relationships. For example, if an outer moraine crest yields an average ¹⁰Be age of 10 ka based on multiple tightly clustered individual ages, then the inner moraine must be younger than 10 ka, and individual ages ≫ 10 ka from the inner moraine may be reasonably discarded. Similarly, boulders on bedrock within the limits of the moraine of interest provide minimum limiting ages (assuming no inheritance) such that moraine sample ages much younger than those inside ages can be reasonably discarded. We use 2 standard deviations (SD) from the mean of the adjacent feature as a threshold for assigning outliers based on morphostratigraphic relationship.
- 3) Finally, we calculate a reduced chi-squared statistic as described in Balco (2011) to determine whether it is appropriate to calculate a mean feature age based on the distribution of individual ages. The reduced chi-squared statistic (χ^2_R) is defined as:

$$\chi^2_R = \frac{1}{n-1} \sum_{i=1}^n \left[\frac{t_i - \bar{t}_i}{\sigma t_i} \right]^2 \quad (1)$$

where n is number of samples, t_i is the apparent exposure age, \bar{t}_i is the mean exposure age, and σ is the measurement uncertainty. In general, a reduced chi-squared value of ~1 suggests that the spread in ages is likely due to analytical uncertainty, rather than geomorphic processes skewing individual ages, and calculating a mean age is an appropriate way to represent the true feature age. A reduced chi-squared value of ≫ 1 suggests that “geomorphic scatter,” or the altering of ages due to inheritance or geomorphic processes, contributes significantly to the scatter in a set of ages, and calculation of a mean age is not justified. When appropriate, we calculate a mean age and report ±1 SD as the feature age uncertainty.

3.4. Radiocarbon dating

At Narpaing Moraine, we collected fragments of terrestrial moss (*Polytrichum*, identified by G. Miller) in foreset beds of a perched

delta formed in a former lake, presumably dammed by the glacier advance that formed the outer Narpaing Moraine (Fig. 2). The age of the macrofossil provides an additional constraint on the timing of cirque glacier advance. The moss fragments were sonicated in deionized water and freeze-dried before undergoing acid-base acid pretreatment and conversion to graphite at the INSTAAR Laboratory for AMS Radiocarbon Preparation and Research. Radiocarbon measurements were made at the UC Irvine AMS facility and calibrated using CALIB 7.1 (Stuiver et al., 2018) with the IntCal13 calibration curve (Reimer et al., 2013).

3.5. Numerical modeling

To explore the possible role of ice dynamics in moraine formation, we crafted a numerical model that quantitatively captures the effect of trunk-tributary disconnection during deglaciation in the Sulung–Narmak valley. We utilize a 1D model characterizing flow along a flowline that includes the tributary profile and its trajectory subsequent to joining the trunk glacier. The effect of the junction is to reduce the width of the tributary glacier. One can see this pinching effect in medial moraine patterns on present glaciers. To first order, the degree of pinching reflects the ratio of ice discharge in tributary and trunk glaciers—the smaller the contribution from the tributary, the greater the reduction in the width (W) of the tributary ice as it joins the trunk. We mimic this effect by reducing the width over a distance that is scaled by the width of the tributary. The effect is simply captured in a 1D flowline model by including variable width in the conservation of ice statement (e.g., Anderson et al., 2006):

$$\frac{\partial H}{\partial t} = b - \frac{1}{W} \frac{\partial QW}{\partial x} = b - \left[\frac{\bar{Q}}{W} \frac{\partial W}{\partial x} + \frac{\partial \bar{Q}}{\partial x} \right] \quad (2)$$

where H is ice thickness, t is time, b is annual mass balance, Q is ice discharge, and x is distance along flow. Operationally, the overbar denotes the mean value within a numerical cell. In the absence of variation in width, the first term in brackets vanishes and we retrieve the simplest flowline model.

At steady state, the effect of a width reduction is to enhance the thickness of the ice, as ice discharge along the flowline must reflect the integral of the ice discharge. Reductions in width must be taken up by increases in Q , which will be accommodated by both an increase in ice thickness and speed.

We ran this numerical model along an elevation profile extracted from the Sulung cirque valley–Narmak trough digital elevation model (Fig. 2), approximating paleo-flowlines based on modern topography and glacial landforms. We impose a climate history that allows the tributary glacier to first grow past the tributary junction, at which point its width is restricted. We then impose a rise in the ELA that promotes trunk glacier retreat past the tributary confluence, at which time the width restriction on the tributary ice is removed. While this 1D flowline model and simplified climate history do not represent the true history of this tributary-trunk pair, the numerical simulation nonetheless captures what we argue is the essence of the glacier response to disconnection.

4. Results

4.1. Cosmogenic radionuclide ages

4.1.1. Fiord ^{10}Be ages

Three erratic boulder samples in outer Okoa Bay yielded ^{10}Be ages of 11.1 ± 0.3 , 11.4 ± 0.2 , and 13.0 ± 0.2 ka (Fig. 1b, Table 2). Because of the proximity (<20 m) of the samples, we expect their

true exposure timing to be the same. Based on the normal kernel density estimate and reduced chi-squared statistic, the oldest age was removed as an outlier. The remaining two ages produce a mean age of 11.2 ± 0.2 ka (Fig. 1). At Maktak Fiord, three erratic boulder samples produced ages of 10.6 ± 0.2 , 10.7 ± 0.2 , and 11.4 ± 0.3 ka, with no apparent outliers (Fig. 1c, Table 2). The three ages yield a mean age of 10.9 ± 0.4 ka (Fig. 1).

4.1.2. Early Holocene moraine ^{10}Be and ^{14}C ages

In Sulung Valley, five ages from the outermost left lateral moraine range from 9.3 ± 0.3 to 19.8 ± 0.5 ka (Table 2, Figs. 2, 4 and 5). Three of these ages are older than 13 ka, likely predating deglaciation of major valleys in the region (Young et al., 2020a); because this outermost moraine partially cross-cuts the Narmak Trough right lateral moraine, and because the old ages do not cluster well, they likely reflect varying levels of inheritance. The three outliers from this moraine, with ^{10}Be ages of 16.9 ± 0.5 , 13.7 ± 0.4 , and 19.8 ± 0.5 ka, were subsequently dated with *in situ* ^{14}C , yielding ages of 9.3 ± 0.8 , 8.7 ± 0.9 , and 9.5 ± 1.0 ka, respectively (Fig. 4, Table 3). The combined ^{10}Be ($n = 2$) and *in situ* ^{14}C ages ($n = 3$) from outer Sulung moraine result in a mean age of 9.2 ± 0.3 ka. Six ages from the inner left lateral moraine range from 8.4 ± 0.3 to 9.8 ± 0.3 ka, yielding a mean age of 9.0 ± 0.5 ka (Table 2, Figs. 2, 4 and 5).

In Narmak Trough, we found no suitable boulders on the outer Narmak Moraine. Four samples from the inner left lateral moraine crest produced ages between 8.1 ± 0.4 and 9.2 ± 0.4 ka (Table 2, Figs. 2 and 5) with no outliers. Four additional samples taken from large boulders resting on bedrock inside of the inner moraine range in age from 8.9 ± 0.3 to 84.1 ± 1.6 ka. Two outliers (10.4 ± 0.7 and 84.1 ± 1.6 ka) were removed because they were >2 SD older than the mean of the moraine crest samples, which are morphostratigraphically older. The remaining two ages (8.9 ± 0.3 and 9.2 ± 0.5 ka) statistically overlap with the four moraine crest samples, so we combined the six ages, which results in a mean age of 8.8 ± 0.4 ka.

In Narpaing Valley, four ages from the outer end moraine range from 7.6 ± 0.6 ka to 17.2 ± 0.9 ka (Table 2, Figs. 2 and 5). After removal of one old outlier (17.2 ± 0.9 ka) based on the normal kernel density estimate, the remaining three ages cluster well and yield a mean age of 8.1 ± 0.4 ka. Six ages from the inner left lateral/end moraine range from 7.1 ± 0.3 to 10.4 ± 0.4 ka (Table 2, Figs. 2 and 5). Because two of the ages (10.0 ± 0.4 and 10.4 ± 0.4 ka) are significantly (>2 SD) older than the mean age of the outer moraine, these ages are removed as outliers. The remaining ages range from 7.1 ± 0.3 to 8.7 ± 0.4 ka, and the resulting value is 4.5. In this case, we choose not to calculate a mean age because of the probable incorporation of geologic uncertainty, and instead present the full range of ages in subsequent interpretations. The moss fragments from perched delta yielded a radiocarbon age of 9.06 ± 0.06 cal BP (Fig. 2, Table 4), which we interpret as a maximum limiting age for the outer Narpaing Moraine because the plant material is reworked.

In Qik valley, four moraine boulder samples produced ages between 7.8 ± 0.2 and 64.4 ± 1.0 ka (Table 2, Figs. 2 and 5). Two old outliers, 14.1 ± 0.3 and 64.4 ± 1.0 ka, were removed from further interpretation. The remaining two ages yield a mean age of 8.0 ± 0.2 ka.

5. Discussion

5.1. Identifying inheritance and other uncertainties in ^{10}Be ages

Most of the features we dated produced at least some boulders with substantial levels of inherited ^{10}Be , totaling 28% of all samples. This is a common challenge in settings with extensive cold-based

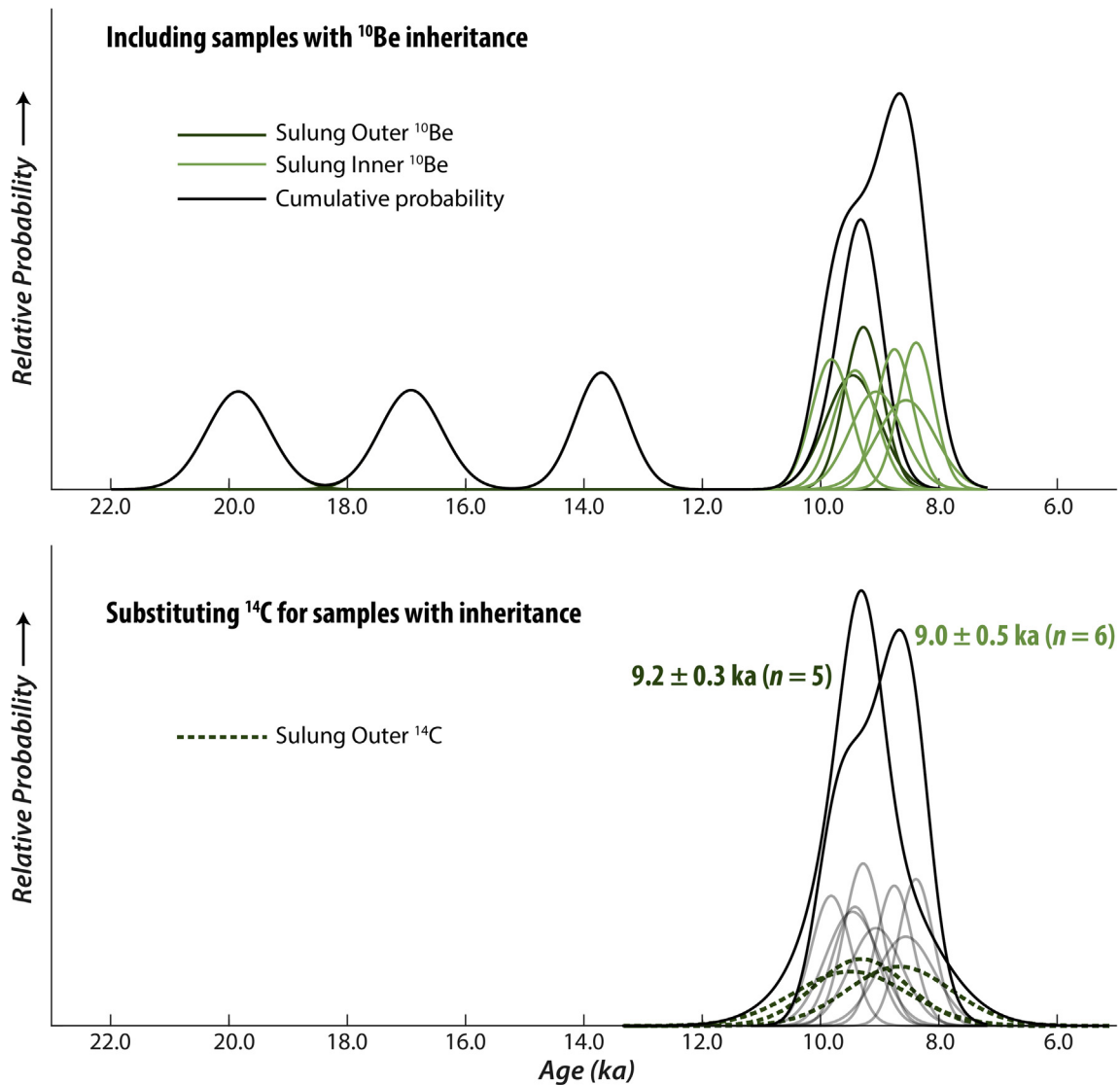


Fig. 4. Normal kernel density estimates for Sulung outer and inner moraines. Top panel incorporates all ^{10}Be ages, including three outliers from the outer crest. Bottom panel incorporates three *in situ* ^{14}C ages instead of the anomalously old ^{10}Be ages. Feature ages are reported as mean \pm 1 SD.

ice, including Baffin Island, because previously accumulated cosmogenic radionuclides are often incompletely eroded from rock surfaces during glacial periods (Corbett et al., 2016a; Miller et al., 2002). The proportion of our samples with inheritance (28%) agrees well with a previous study that found 31% of 635 published ^{10}Be ages from Baffin Island were affected by inheritance (Young et al., 2016). With samples containing high levels of inherited ^{10}Be from the Sulung outer moraine, we demonstrate the utility of *in situ* ^{14}C to clarify the timing of moraine formation (Fig. 4). ^{14}C ages between 8.7 and 9.5 ka fit well with the remaining ^{10}Be ages from the same moraine, substantially increasing confidence in the average moraine age of 9.2 ± 0.3 ka.

In addition, geomorphic processes that take place after deposition of a moraine can affect boulders' radionuclide inventories (Crump et al., 2017; Putkonen and O'Neal, 2006). Specifically, ice-core melt-out, moraine surface lowering, and diffusion of sharp moraine crests can result in the rolling of individual boulders, which produces spuriously low ^{10}Be inventories. These processes take place most prominently early in the history of a moraine, so

the resulting too-young ages may not be obvious enough to remove from mean age calculations. Furthermore, exhumation of boulders near the moraine crest is possible, particularly in settings with active permafrost processes as is the case at our sites. The younger (<8 ka) ^{10}Be ages from the Narpaing inner moraine likely result from these post-depositional processes, particularly given the lack of other <8 ka moraine ages from the region.

The influence of both too-old and too-young outliers from these drivers of geologic scatter reduce the precision of feature mean ages. As a result, for the sites with multiple nested moraine crests, the estimated ages of outer and inner moraines are statistically indistinguishable: 9.2 ± 0.3 ka and 9.0 ± 0.5 ka at Sulung and 8.1 ± 0.4 ka and 7.1–8.7 ka at Narpaing. The data cannot definitely distinguish between the moraines forming some hundreds of years apart due to distinct cooling episodes with some retreat in the intervening warm period, versus both crests forming within decades as a result of interannual variability or unsteady retreat (Anderson et al., 2014).

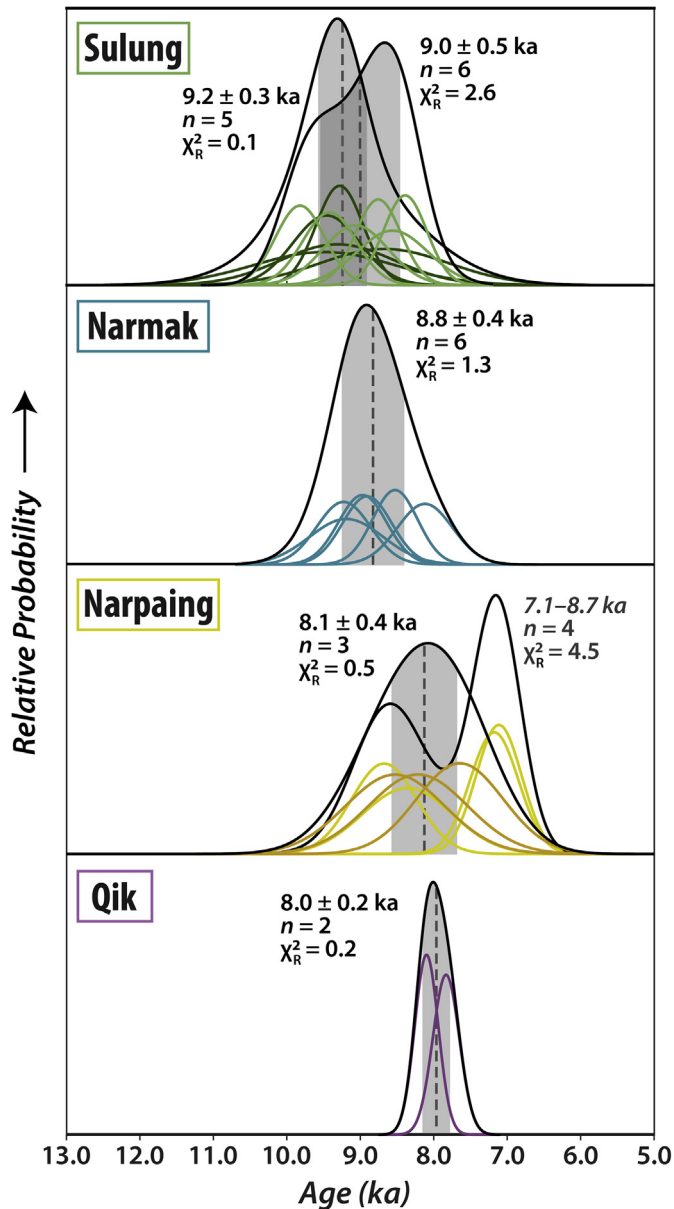


Fig. 5. Normal kernel density estimates for moraine ages. Colored lines each represent an individual sample age distribution, with the darker shade lines indicating samples from the outer crest where applicable. Black lines are cumulative kernel density functions for a moraine crest. Dashed vertical line and gray shading are mean \pm 1 SD for a moraine crest if calculated. (For interpretation of the references to color in this figure legend, the reader is referred to the Web version of this article.)

5.2. Alignment of moraine ages with known abrupt climate events

Erratic boulder ages from Okoa Bay and Maktak Fiord indicate that LIS outlet glaciers in this region retreated past fiord mouths by \sim 11 ka (Fig. 1). We note that the Okoa Bay erratic boulder average age (11.2 ± 0.2 ka) predates a radiocarbon date on marine shells

from a nearby ice-proximal delta (9.1 ± 0.9 ka [\pm 2 SD]) that should also constrain the timing of deglaciation (Briner et al., 2009; Miller, 1973). However, the ^{10}Be ages overlap (within uncertainties) with the average ^{10}Be age for a lateral moraine farther up-fiord (11.8 ± 0.4 ka; Fig. 1a). Erratics on lateral moraines from within Narpaing Fiord date to \sim 10.4 and 9.3 ka, documenting progressive deglaciation and suggesting that major LIS outlets likely responded to early Holocene cooling events as argued by Young et al. (2020a).

Following regional deglaciation, moraine crests formed by cirque glaciers and ice cap outlets stabilized at \sim 9.2 and 9.0 ka (Sulung moraines), \sim 8.8 ka (Narmak inner moraine), \sim 8.1 ka (Narpaing outer moraine), and \sim 8.0 ka (Qik moraine), with the less well-constrained Narpaing inner moraine bracketed between 7.1 and 8.7 ka and corroborated by a limiting radiocarbon age of 9.1 ka. Taken together, mean ages of each moraine statistically overlap (within 1 SD) with either the 9.3 or 8.2 ka events, both of which are well-defined cold periods in Greenland ice core records (Fig. 5) (Kobashi et al., 2007; Rasmussen et al., 2007; Thomas et al., 2007) and are further recorded in a variety of terrestrial temperature proxy records (e.g. Axford et al., 2009; Briner et al., 2016). Robust geologic evidence indicates that the 8.2 ka event was caused by freshwater fluxes through Hudson Strait that temporarily reduced or shut down AMOC with hemispheric-scale climate impacts (Barber et al., 1999; Clarke et al., 2004; Jennings et al., 2015; Kleiven et al., 2008; LeGrande et al., 2006; Morrill et al., 2014). The 9.3 ka event, although less thoroughly studied, was likely caused by similar freshwater forcing (Came et al., 2007; Fleitmann et al., 2008; Jennings et al., 2015) (Fig. 6). Our moraine ages corroborate a growing number of glacier chronologies from the Baffin Bay region that have pointed to the expansion of glaciers and ice sheets in response to the freshwater-forced 9.3 and 8.2 ka events, which likely featured cold summers given the similarity response time for both LIS and local ice features (Briner et al., 2009; Young et al., 2020a, 2012, 2013a). Given age uncertainties in both the marine records and in moraine exposure dating, however, the alignment of these discharge events with glacier expansion is imperfectly resolved.

Although the moraines dated here likely formed between \sim 9.3 and 8.0 ka, the uncertainty of these moraine ages is still too large to unequivocally tie individual moraine-building events to $<$ 200-year-long cooling events (Rasmussen et al., 2007). We thus assess the exposure age results in the context of additional considerations, including 1) millennial-scale climate trends in the Baffin Bay region during the early Holocene, 2) inferences about regional vs larger-scale circulation-driven cooling, and 3) the dynamic response of local tributary glaciers to regional deglaciation.

5.3. Changing ocean conditions in Baffin Bay

In addition to well-known cooling episodes caused by distinct freshwater outburst through Hudson Strait, early Holocene climate in the Baffin Bay region was likely influenced by background meltwater input into the region via ongoing deglaciation of the Laurentide, Innuitian and Greenland ice sheets (Bennike and Björck, 2002; Briner et al., 2009; Dyke, 1999; Jennings et al., 2011; Kaplan and Miller, 2003; Lloyd et al., 2005; Sheldon et al., 2016). Marine records from outer Disko Trough in eastern Baffin Bay

Table 4
Plant radiocarbon dating details.

Lab ID	Sample type	Conventional age (^{14}C yr BP)	Uncertainty (^{14}C yrs)	Median calibrated age (cal yr BP) ^a	-2σ (cal yr BP)	$+2\sigma$ (cal yr BP)
CURL-20189	Terrestrial moss	8130	\pm 25	9060	9009	9123

^a Calibrated using CALIB 7.1 (Stuiver et al., 2018) with the IntCal13 calibration curve (Reimer et al., 2013).

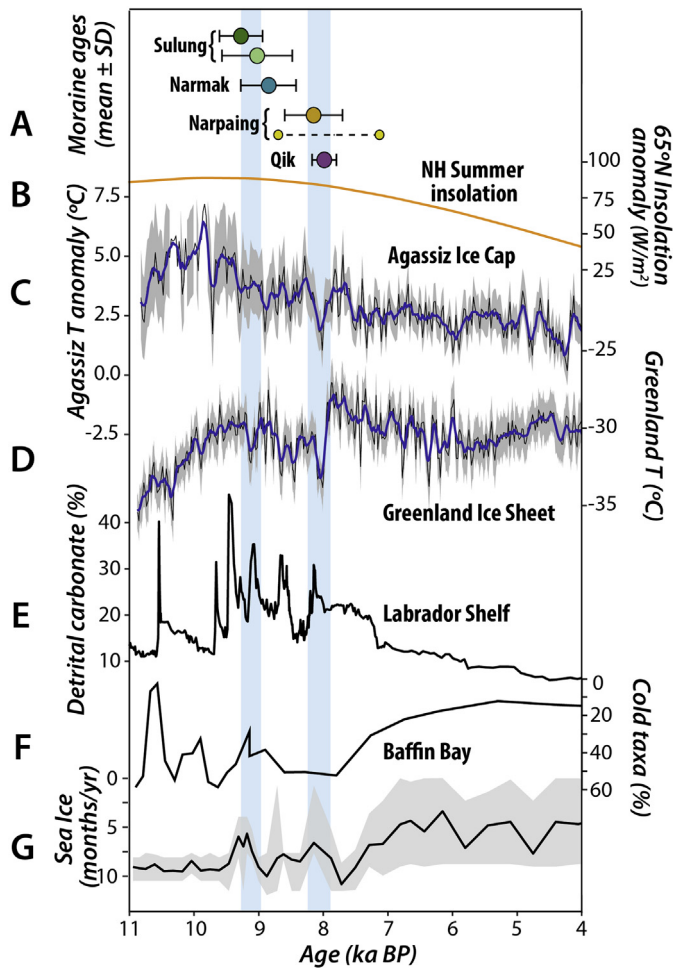


Fig. 6. Moraine ages within the context of regional climate records. A) Mean and standard deviation of moraine crests from this study (Narpaing Inner moraine is shown as full range of ages, as described in text). B) Summer insolation anomaly for 65°N (Berger, 1978). C) Temperature anomaly based on $\delta^{18}\text{O}$ measured in Agassiz ice core record (Lecavalier et al., 2017). D) Central Greenland temperature estimates from argon and nitrogen isotopes in gas from GISP2 (Kobashi et al., 2017). E) Detrital carbonate weight percent in marine sediment core 2236 from the Labrador shelf (Jennings et al., 2015). F) Cold foraminiferal taxa percent in marine sediment core CC70 from Disko Trough (Jennings et al., 2014). G) Estimated duration of sea ice cover in Disko Trough based on dinocyst assemblages in core CC70 (Gibb et al., 2015). Vertical blue bars represent approximate timing of 9.3 and 8.2 ka events. (For interpretation of the references to color in this figure legend, the reader is referred to the Web version of this article.)

suggest that ocean conditions between ~12 and 8 ka were cold but variable and characterized by a prolonged ice-covered season (Fig. 6) (Gibb et al., 2015; Jennings et al., 2014). Foraminiferal assemblages indicate marked warming after ~7.8 ka (Jennings et al., 2014; Lloyd et al., 2005), which is corroborated by a dinocyst-inferred temperature reconstruction from an adjacent core that shows pronounced summer sea-surface temperature warming starting before ~7.4 ka (Gibb et al., 2015). Both cores suggest sea-ice cover between ~8 and 11 months per year prior to 8 ka. Together, these records paint a cohesive early Holocene picture of a cold, ice-filled Baffin Bay. Ice and meltwater discharge events from around Baffin Bay and through Hudson Strait, as well as a series of large volcanic eruptions (Kobashi et al., 2017), likely exacerbated these cold baseline conditions at irregular intervals.

Today, eastern Baffin Bay is influenced by the relatively warm West Greenland Current (WGC; Fig. 1) (Tang et al., 2004). A reduced or absent WGC would result in colder summers along West

Greenland and more persistent sea ice cover, which would likely depress summer temperatures on eastern Baffin Island as well. Paleoceanographic records from Disko Bugt indicate that the WGC strengthened markedly in the centuries following 8 ka (Lloyd et al., 2005; Perner et al., 2013). Early Holocene intensification of the WGC is also suggested by the presence of warm boreal mollusc taxa on West Greenland between ~9 and 5 ka (Funder and Weidick, 1991) and a shift to a warmer foraminiferal assemblage on the Baffin Island shelf between ~8.5 and 6 ka (Osterman and Nelson, 1989). Together, these marine records suggest that cool conditions in the earliest Holocene were in part due to low ocean heat transport relative to modern oceanographic conditions.

A post-8 ka increase in WGC strength and associated amelioration of Baffin Bay conditions may have implications for temperatures recorded in central Greenland. As pointed out by Buizert et al. (2018), elevation-adjusted temperature reconstructions from central Greenland and the Agassiz Ice Cap are significantly offset in the early Holocene (Fig. 6). While Agassiz records peak Holocene temperatures at ~10 ka, in line with the summer insolation maximum (Lecavalier et al., 2017), Greenland ice core records indicate depressed temperatures during this period, with peak warmth occurring later—generally after 8 ka (Fig. 6) (Buizert et al., 2018; Kobashi et al., 2017). We hypothesize that this difference may in part be due to cold sea surface conditions in Baffin Bay prior to 8 ka, which would have both cooled Greenland and decreased the regional equilibrium line altitude (ELA) of glaciers and ice caps. Agassiz Ice Cap, on the other hand, may have been less influenced by variable ocean heat transport; its temperature history primarily reflects the summer insolation signal. With abrupt rejuvenation of AMOC at the end of the 8.2 ka event, and with it a strengthening of the WGC, Greenland temperatures would have fallen more in line with those at Agassiz, and glaciers in the Baffin Bay region would have retreated.

Prior to 8 ka, relatively cold sea surface temperatures and a prolonged sea-ice season would have contributed to depressed summer temperatures on eastern Baffin Island. In response, coastal glaciers would have advanced due to reduced summer ablation (i.e., shortened melt season). A millennial-scale period of cool summers would have primed these glaciers for culminating advances that likely occurred during short-lived periods of reduced overturning circulation at 9.3 and 8.2 ka.

5.4. Regional versus hemisphere-scale cooling

The alignment of moraine ages, within limits of the dating method, with both the 9.3 and 8.2 ka events prompts questions about the comparability of the two abrupt climate events. 150–200 years of cool summers and low accumulation beginning at 8.2 ka is a consistent feature of Greenland ice core records, and evidence of cooling and/or drying has been identified in proxy records from a variety of settings around the Northern Hemisphere (e.g., Alley et al., 1997; Davis et al., 2009; Geirsdóttir et al., 2013; Kobashi et al., 2007; Rasmussen et al., 2007). In contrast, excursions in Greenland ice core records at ~9.3 ka are shorter-lived and less spatially consistent (Rasmussen et al., 2007); evidence of cooling and/or drying from distal sites around the Northern Hemisphere is more sparse (summarized in Fleitmann et al., 2008). Agassiz Ice Cap records show clearer cooling at 8.2 ka than at 9.3 ka, corroborating the more widespread nature of the 8.2 ka event (Fisher et al., 1995; Lecavalier et al., 2017). The less spatially extensive cooling event at 9.3 ka may have thus been caused by more localized factors, including freshwater or ice fluxes into Baffin Bay that exacerbated summer cooling and perhaps shut down the already-weak WGC, without the larger-scale AMOC reduction that likely characterized the 8.2 ka event.

The lack of an 8.2 ka moraine in many glacial valleys of eastern Baffin Island suggests that locally, cooling at 8.2 ka was not significantly more pronounced than previous coolings. If glaciers there generally advanced due to 8.2 ka cooling, then at many sites, including Sulung and Narmak valleys, this advance was not more extensive than previous early Holocene end moraine positions and either did not result in moraine formation or was less extensive than subsequent late Holocene advances. Indeed, a chironomid-based temperature reconstruction from Lake CF8 on northeastern Baffin Island indicates similarly cool conditions for two abrupt events that roughly align with the 9.3 and 8.2 ka events (Axford et al., 2009). Alternatively, non-climatic factors, including deglacial ice dynamics, could have played an important role in pre-8.2 ka moraine formation (see section 5.5). Assessing the differences in the precise cause and climatic impacts of these two short-lived cooling events offers an opportunity to better understand the varying degrees of overturning circulation disruption. Additional high-resolution, well-dated climate records from the Baffin Bay region will help elucidate the nature of these enigmatic events.

5.5. Non-climatic factors: the role of initial conditions and trunk valley ice buttressing

The distinct physiographic settings of the four study sites prompts us to critically explore potential mechanisms that may help explain similar moraine records across the region. In particular, Sulung Valley is a directly south-facing cirque that currently holds no ice because of its southern aspect; high summer insolation

in the early Holocene would have exacerbated this contrast with its neighboring north-facing cirques, including the valley associated with Narmak Moraine. While it is possible that the mass balance of the Sulung Valley paleo-glacier was influenced by redistributed snow (wind-blown or avalanched) (e.g., Hoffman et al., 2007; Kuhn, 2003), another important consideration is its mechanistic relationship with trunk valley ice in Narmak Trough.

In the buildup to full glacial conditions, side valley glaciers coalesced with Narmak Trough ice; this configuration would have resulted in a thickening of the tributary glaciers because of the buttressing effect of trunk valley ice (Anderson et al., 2006; MacGregor et al., 2000). At tributary junctions, an inflowing glacier will thicken such that its elevation matches that of the trunk glacier. Down-valley of the tributary–trunk junction, the tributary is confined to a narrower width (W) than its up-valley width (W_0), maintaining steady ice discharge in its over-thickened configuration as illustrated schematically in Fig. 7a. Narmak Trough is a relatively low-angle valley between steep steps that connect it to Maktak and Narpaing fiords on either end. Trough ice may have thus exhibited threshold sensitivity to a small increase in ELA, disappearing rapidly as fiord ice retreated and thinned between ~11 and 9 ka. Fiord ice may have lost mass rapidly due to calving even in the absence of climatic forcing. As Narmak Trough ice thinned, the profiles of tributary glaciers would have adjusted to the absence of buttressing ice by both thinning and advancing into the newly ice-free trough (Fig. 7b).

Our numerical model captured one simplified version of this scenario along the Sulung paleo-flowline. We initiate a tributary

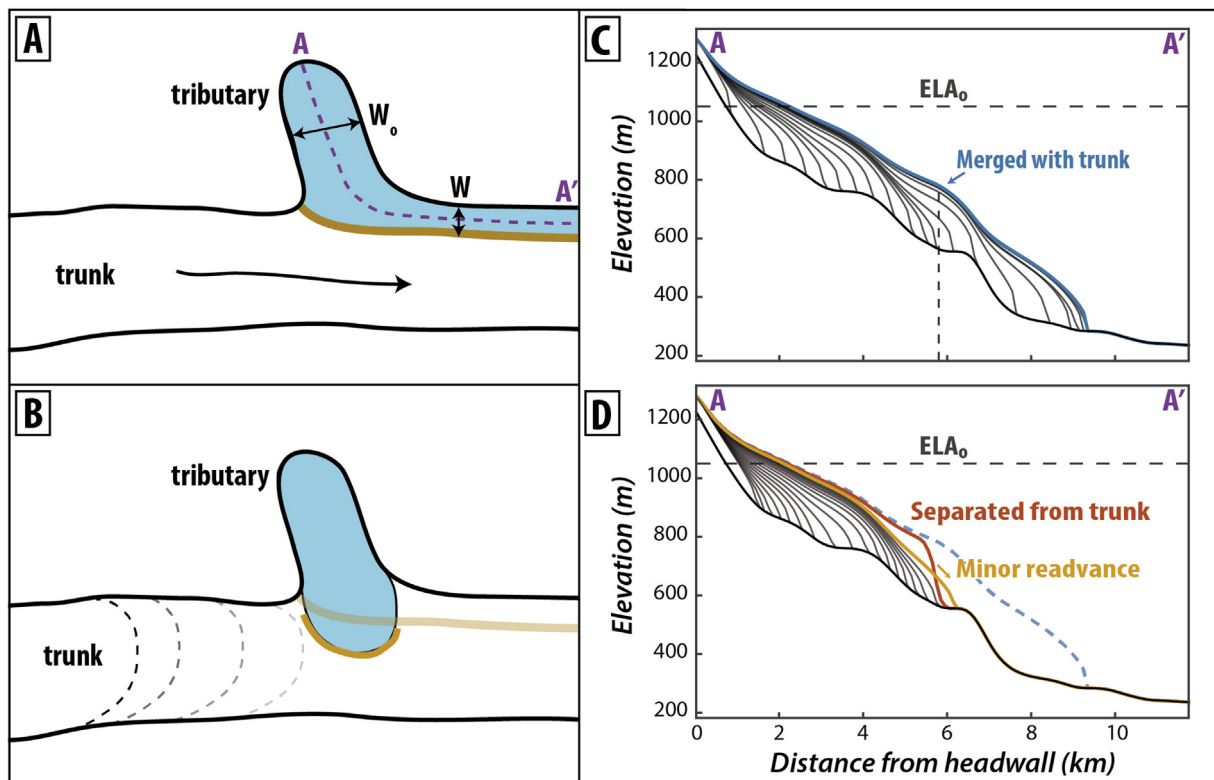


Fig. 7. Schematic (A and B) and numerical model output (C and D) depictions of tributary junction geometries. A) While trunk ice exists, tributary glacier thickens and is confined to a narrower width (W) downvalley of the junction than its up-valley width (W_0). A medial moraine forms at the junction (brown stripe). B) Following trunk deglaciation, tributary glacier thins and extends, depositing a moraine (brown stripe) in the valley bottom. C) Numerical model output depicting tributary glacier extent along an elevation profile A to A'. Each gray curve is the glacier profile at a given time step. Under initial climate forcing (ELA_0), the tributary glacier grows and merges with trunk ice at the position noted with dashed line, resulting in enhanced thickness and length. D) Following a rise in ELA, the tributary glacier retreats and separates from trunk ice (orange profile), then thins and advances slightly in the following timestep (yellow profile) before retreating fully. (For interpretation of the references to color in this figure legend, the reader is referred to the Web version of this article.)

Sulung glacier whose width is restricted at the point of convergence with trunk ice, which thus enhances ice thickness (Fig. 7c). A sinusoidal increase in the ELA drives glacier retreat past the width-restricted point. This releases the enhanced ice thickness, causing the glacier to readvance on the order of ~200 m into the valley temporarily (Fig. 7d). The ELA then continues to rise, further reducing the ice discharge, and the terminus of the tributary retreats out of the trunk valley.

Although a lack of datable boulders on the outer Narmak Moraine precludes full chronologic control, the similarity in ages of Sulung and Narmak moraines—despite their aspect and elevation differences—hints that this mechanistic response to trough deglaciation may have played a role in the formation of those moraines. In addition, the lack of an 8.2 ka moraine at both of these sites lends further support to the notion that the initial configuration of this ice complex predisposed tributary glaciers to extending and depositing moraines in the ~9.3 to 8.8 ka window, partially as a mechanistic response to thinning of buttressing trough ice. The presence of nested moraine crests at both sites suggests that if a debuttressing-driven profile adjustment drove an initial advance, climate conditions allowed for the glaciers to remain extended long enough to build two distinct moraines—as part of glacier length fluctuations in a variable climate (Anderson et al., 2014), or due to unsteady retreat.

6. Conclusions

Four glacial valleys on eastern Baffin Island feature moraines deposited during the unstable climate of the early Holocene in the North Atlantic region. Using cosmogenic ^{10}Be and *in situ* ^{14}C , we show that these moraines were formed between 9.2 and 8.0 ka, statistically overlapping with known abrupt cooling events at 9.3 and 8.2 ka. Individual moraine crests date to 9.2 ± 0.3 ka, 9.0 ± 0.5 ka, 8.8 ± 0.4 ka, 8.1 ± 0.4 ka, and 8.0 ± 0.2 ka, with an additional crest deposited between ~7.1 and 8.7 ka. In addition to distinct centennial-scale, freshwater-forced cooling episodes at 9.3 and 8.2 ka, baseline sea-surface conditions in Baffin Bay prior to 8 ka were relatively cold due to high background rates of ice and meltwater discharge from ice streams of the waning Laurentide and Greenland ice sheets, as well as reduced heat transport by a relatively weak WGC. Glaciers near the coast of Baffin Bay, such as those that built the moraines in this study, may have thus been primed for culminating advances during the brief 9.3 and 8.2 ka cold excursion windows. Thinning of Narmak trunk-valley ice immediately preceding Narmak and Sulung moraine formation, to which these glaciers were tributaries, may have caused a dynamic adjustment of the over-thickened tributary glaciers and contributed to their subsequent minor extension into Narmak Trough. These new chronologic constraints confirm that cirque glaciers and ice cap outlets responded to early Holocene climate oscillations and, more broadly, to deglacial dynamics in the Baffin Bay region.

Data availability

Datasets related to this article can be found at <https://doi.org/10.18739/A2ST7DX28>, hosted at the NSF Arctic Data Center online repository.

CRedit authorship contribution statement

Sarah E. Crump: Investigation, Formal analysis, Data curation, Writing - original draft, Visualization. **Nicolás E. Young:** Conceptualization, Investigation, Writing - review & editing, Funding acquisition. **Gifford H. Miller:** Conceptualization, Investigation, Writing - review & editing, Supervision, Funding acquisition.

Simon L. Pendleton: Investigation, Writing - review & editing, Visualization. **Joseph P. Tulenko:** Investigation, Writing - review & editing. **Robert S. Anderson:** Investigation, Writing - review & editing, Visualization. **Jason P. Briner:** Conceptualization, Investigation, Writing - review & editing, Supervision, Funding acquisition.

Acknowledgements

We gratefully acknowledge the Qikiqtaani Inuit and government of Nunavut and Canada for field site access (Nunavut Research Institute license # 02 021 15 R-M; Auyuittuq National Park research permit # ANP-2013-14193). We thank Gordie Audlakiak, Mina Kunilusie, and Allan and Lisa Kunilusie for field support, as well as CH2MHill Polar Services for logistical support. This work was supported by the National Science Foundation Arctic Natural Sciences program (Awards #1417675 to NEY; #1417783 to JPB; #1418040 to GHM). Contributions of S.E.C. were supported by a National Science Foundation Graduate Research Fellowship (award #1144083). This is Lamont-Doherty Earth Observatory contribution #8421.

References

- Alley, R.B., Agustsdottir, A.M., 2005. The 8k event: cause and consequences of a major Holocene abrupt climate change. *Quat. Sci. Rev.* 24, 1123–1149. <https://doi.org/10.1016/j.quascirev.2004.12.004>.
- Alley, R.B., Marotzke, J., Nordhaus, W.D., Overpeck, J.T., Peteet, D.M., Pielke, R.A.J., Pierrehumbert, R.T., Rhines, P.B., Stocker, T.F., Talley, L.D., Wallace, J.M., 2003. Abrupt climate change. *Science* 299, 2005–2011. <https://doi.org/10.1126/science.1101366>.
- Alley, R.B., Mayewski, P.A., Sowers, T., Stuiver, M., Taylor, K.C., Clark, P.U., 1997. Holocene climatic instability: a prominent, widespread event 8200 yr ago. *Geology* 25, 483. [http://10.1130/0091-7613\(1997\)025%3C0483:HCIAPW%3E2.3.CO;2](http://10.1130/0091-7613(1997)025%3C0483:HCIAPW%3E2.3.CO;2).
- Anderson, L.S., Roe, G.H., Anderson, R.S., 2014. The effects of interannual climate variability on the moraine record. *Geology* 42, 55–58. <https://doi.org/10.1130/G34791.1>.
- Anderson, R.S., Molnar, P., Kessler, M.A., 2006. Features of glacial valley profiles simply explained. *J. Geophys. Res.: Earth Surface* 111, 1–14. <https://doi.org/10.1029/2005JF000344>.
- Andrews, J.T., Ives, J.D., 1978. “Cockburn” nomenclature and the late quaternary history of the eastern Canadian arctic. *Arct. Alp. Res.* 10, 617–633.
- Axford, Y., Briner, J.P., Miller, G.H., Francis, D.R., 2009. Paleoclimatic evidence for abrupt cold reversals during peak Holocene warmth on Baffin Island, Arctic Canada. *Quater. Res.* 71, 142–149. <https://doi.org/10.1016/j.yqres.2008.09.006>.
- Balco, G., 2017. Production rate calculations for cosmic-ray-muon-produced ^{10}Be and ^{26}Al benchmarked against geological calibration data. *Quat. Geochronol.* 39, 150–173. <https://doi.org/10.1016/j.quageo.2017.02.001>.
- Balco, G., 2011. Contributions and unrealized potential contributions of cosmogenic-nuclide exposure dating to glacier chronology, 1990–2010. *Quat. Sci. Rev.* 30, 3–27. <https://doi.org/10.1016/j.quascirev.2010.11.003>.
- Balco, G., Stone, J.O., Lifton, N.A., Dunai, T.J., 2008. A complete and easily accessible means of calculating surface exposure ages or erosion rates from ^{10}Be and ^{26}Al measurements. *Quat. Geochronol.* 3, 174–195. <https://doi.org/10.1016/j.quageo.2007.12.001>.
- Barber, D.C., Dyke, A., Hillaire-Marcel, C., Jennings, A.E., Andrews, J.T., Kerwin, M.W., Bilodeau, B., McNeely, R., Southon, J., Morehead, M.D., Gagnon, J.-M., 1999. Forcing of the cold event of 8,200 years ago by catastrophic drainage of Laurentide lakes. *Nature* 400, 344–348. <https://doi.org/10.1038/22504>.
- Bennike, O., Björck, S., 2002. Chronology of the last recession of the Greenland ice sheet. *J. Quat. Sci.* 17, 211–219. <https://doi.org/10.1002/jqs.670>.
- Bond, G., 1997. A pervasive millennial-scale cycle in North Atlantic Holocene and glacial climates. *Science* 278, 1257–1266. <https://doi.org/10.1126/science.278.5341.1257>.
- Briner, J.P., Davis, P.T., Miller, G.H., 2009. Latest Pleistocene and Holocene glaciation of Baffin Island, Arctic Canada: key patterns and chronologies. *Quat. Sci. Rev.* 28, 2075–2087. <https://doi.org/10.1016/j.quascirev.2008.09.017>.
- Briner, J.P., Mckay, N.P., Axford, Y., Bennike, O., Bradley, R.S., Vernal, A. De, Fisher, D., Francus, P., Miller, G., Rouston, C., Wagner, B., 2016. Holocene climate change in Arctic Canada and Greenland. *Quat. Sci. Rev.* 147, 340–364.
- Briner, J.P., Overeem, I., Miller, G., Finkel, R., 2007. The deglaciation of Clyde Inlet, Northeastern Baffin Island, Arctic Canada. *J. Quat. Sci.* 22, 223–232. <https://doi.org/10.1002/jqs>.
- Broecker, W.S., 2000. Abrupt climate change: causal constraints provided by the paleoclimate record. *Earth Sci. Rev.* 51, 137–154. [https://doi.org/10.1016/S0012-8252\(00\)00019-2](https://doi.org/10.1016/S0012-8252(00)00019-2).

- Broecker, W.S., 1991. The great ocean conveyor. *Oceanography* 4, 79–89.
- Buizert, C., Keisling, B.A., Box, J.E., He, F., Carlson, A.E., Sinclair, G., DeConto, R.M., 2018. Greenland-wide seasonal temperatures during the last deglaciation. *Geophys. Res. Lett.* 45, 1905–1914. <https://doi.org/10.1002/2017GL075601>.
- Came, R.E., Oppo, D.W., McManus, J.F., 2007. Amplitude and timing of temperature and salinity variability in the subpolar North Atlantic over the past 10 kyr. *Geology* 35, 315–318. <https://doi.org/10.1130/G23455A.1>.
- Chen, Y., Li, Y., Wang, Y., Zhang, M., Cui, Z., Yi, C., Liu, G., 2015. Late Quaternary glacial history of the Karlik Range, easternmost Tian Shan, derived from ^{10}Be surface exposure and optically stimulated luminescence datings. *Quat. Sci. Rev.* 115, 17–27. <https://doi.org/10.1016/j.quascirev.2015.02.010>.
- Clark, P.U., Pisias, N.G., Stocker, T.F., Weaver, A.J., 2002. The role of the thermohaline circulation in abrupt climate change. *Nature* 415, 863–869.
- Clarke, G.K.C., Leverington, D.W., Teller, J.T., Dyke, A.S., 2004. Paleohydraulics of the last outburst flood from glacial Lake Agassiz and the 8200 BP cold event. *Quat. Sci. Rev.* 23, 389–407. <https://doi.org/10.1016/j.quascirev.2003.06.004>.
- Corbett, L.B., Bierman, P.R., Davis, P.T., 2016a. Glacial History and Landscape Evolution of Southern Cumberland Peninsula, Baffin Island, Canada, Constrained by Cosmogenic ^{10}Be and ^{26}Al . *Geological Society of America Bulletin*.
- Corbett, L.B., Bierman, P.R., Rood, D.H., 2016b. An approach for optimizing in situ cosmogenic ^{10}Be sample preparation. *Quat. Geochronol.* 33, 24–34. <https://doi.org/10.1016/j.quageo.2016.02.001>.
- Corbett, L.B., Young, N.E., Bierman, P.R., Briner, J.P., Neumann, T.A., Rood, D.H., Graly, J.A., 2011. Paired bedrock and boulder ^{10}Be concentrations resulting from early Holocene ice retreat near Jakobshavn Isfjord, western Greenland. *Quat. Sci. Rev.* 30, 1739–1749. <https://doi.org/10.1016/j.quascirev.2011.04.001>.
- Council, N.R., 2002. Abrupt Climate Change: Inevitable Surprises. National Academy Press, Washington, D.C. <https://doi.org/10.17226/10136>.
- Crump, S.E., Anderson, L.S., Miller, G.H., Anderson, R.S., 2017. Interpreting exposure ages from ice-cored moraines: a Neoglacial case study on Baffin Island, Arctic Canada. *J. Quat. Sci.* <https://doi.org/10.1002/jqs.2979>.
- Dansgaard, W., Johnson, S.J., Clausen, H.B., Dahl-Jensen, D., Gundestrup, N.S., Hammer, C.U., Hvidberg, C.S., Steffensen, J.P., Sveinbjörnsdóttir, A.E., Jouzel, J., Bond, G., 1993. Evidence for general instability of past climate from a 250-kyr ice-core record. *Nature* 364, 218–220.
- Davis, P.T., Menounos, B., Osborn, G., 2009. Holocene and latest Pleistocene alpine glacier fluctuations: a global perspective. *Quat. Sci. Rev.* 28, 2021–2033. <https://doi.org/10.1016/j.quascirev.2009.05.020>.
- Donner, J., Jungner, H., 1975. Radiocarbon dating of shells from marine deposits in the Disko Bugt area, West Greenland. *Boreas* 4, 25–45.
- Dugdale, R.E., 1972. The quaternary history of the northern Cumberland Peninsula, Baffin Island, N.W.T. Part III: the late glacial deposits of Sulung and Itdilrin valleys and adjacent parts of the Maktak-Narpaing Trough. *Can. J. Earth Sci.* 9.
- Dyke, A.S., 1999. Last glacial maximum and deglaciation of Devon Island, Arctic Canada: support for an innuitian ice sheet. *Quat. Sci. Rev.* 18, 393–420. [https://doi.org/10.1016/S0277-3791\(98\)00005-5](https://doi.org/10.1016/S0277-3791(98)00005-5).
- Dyke, A.S., Andrews, J.T., Miller, G.H., 1982. Quaternary Geology of Cumberland Peninsula, Baffin Island, District of Franklin.
- Fisher, D.A., Koerner, R.M., Reeh, N., 1995. Holocene climatic records from Agassiz Ice Cap, Ellesmere Island, NWT, Canada. *Holocene* 5, 19–24.
- Fleitmann, D., Mudelsee, M., Burns, S.J., Bradley, R.S., Kramers, J., Matter, A., 2008. Evidence for a widespread climatic anomaly at around 9.2 ka before present. *Paleoceanography* 23, 1–6. <https://doi.org/10.1029/2007PA001519>.
- Funder, S., Weidick, A., 1991. Holocene Boreal molluscs in Greenland—palaeoceanographic implications. *Palaeogeogr. Palaeoclimatol. Palaeoecol.* 85, 123–135.
- Gardner, A., Moholdt, G., Arendt, A., Wouters, B., 2012. Accelerated contributions of Canada's Baffin and Bylot Island glaciers to sea level rise over the past half century. *Cryosphere* 6, 1103–1125. <https://doi.org/10.5194/tc-6-1103-2012>.
- Gardner, A.S., Moholdt, G., Wouters, B., Wolken, G.J., Burgess, D.O., Sharp, M.J., Cogley, J.G., Braun, C., Labine, C., 2011. Sharply increased mass loss from glaciers and ice caps in the Canadian Arctic Archipelago. *Nature* 473, 357–360. <https://doi.org/10.1038/nature10089>.
- Geirsdóttir, Á., Miller, G.H., Larsen, D.J., Ólafsdóttir, S., 2013. Abrupt Holocene climate transitions in the northern North Atlantic region recorded by synchronized lacustrine records in Iceland. *Quat. Sci. Rev.* 70, 48–62. <https://doi.org/10.1016/j.quascirev.2013.03.010>.
- Gibb, O.T., Steinhauer, S., Fréchette, B., de Vernal, A., Hillaire-Marcel, C., 2015. Diachronous evolution of sea surface conditions in the Labrador Sea and Baffin Bay since the last deglaciation. *Holocene* 25, 1882–1897. <https://doi.org/10.1177/0959683615591352>.
- Hoffman, M.J., Fountain, A.G., Achuff, J.M., 2007. 20th-century variations in area of cirque glaciers and glacierets, Rocky Mountain National Park, Rocky Mountains, Colorado, USA. *Ann. Glaciol.* 46, 349–354. <https://doi.org/10.3189/172756407782871233>.
- Jennings, A., Andrews, J., Pearce, C., Wilson, L., Olfasd, S., 2015. Detrital carbonate peaks on the Labrador shelf, a 13–7 ka template for freshwater forcing from the Hudson Strait outlet of the Laurentide Ice Sheet into the subpolar gyre. *Quat. Sci. Rev.* 107, 62–80. <https://doi.org/10.1016/j.quascirev.2014.10.022>.
- Jennings, A.E., Sheldon, C., Cronin, T.M., Francus, P., Stoner, J., Andrews, J.T., 2011. The Holocene history of Nares Strait: transition from glacial bay to Arctic-Atlantic throughflow. *Oceanography* 24, 26–41.
- Jennings, A.E., Walton, M.E., Colm, O.C., Killeather, A., Andrews, J.T., Ortiz, J.D., De Vernal, A., Dowdeswell, J.A., 2014. Paleoenvironments during Younger Dryas-early Holocene retreat of the Greenland ice sheet from outer Disko Trough, central west Greenland. *J. Quat. Sci.* 29, 27–40. <https://doi.org/10.1002/jqs.2652>.
- Johnsen, S.J., Clausen, H.B., Dansgaard, W., Fuhrer, K., Gundestrup, N., Hammer, C.U., Iversen, P., Jouzel, J., Stauffer, B., Steffensen, J.P., 1992. Irregular glacial interstadials recorded in a new Greenland ice core. *Nature* 359, 311–313.
- Kaplan, M.R., Miller, G.H., 2003. Early Holocene deleveling and deglaciation of the Cumberland Sound region, Baffin Island, Arctic Canada. *Geol. Soc. Am. Bull.* 115, 445–462.
- Kleiven, F.H., Kissel, C., Laj, C., Ninnemann, U.S., Richter, T.O., Cortijo, E., 2008. Reduced North Atlantic deep water coeval with the glacial lake Agassiz freshwater outburst. *Science* 319, 60–65.
- Kobashi, T., Menviel, L., Jeltsch-Thömmes, A., Vinther, B.M., Box, J.E., Muscheler, R., Nakaegawa, T., Pfister, P.L., Döring, M., Leuenberger, M., Wanner, H., Ohmura, A., 2017. Volcanic influence on centennial to millennial Holocene Greenland temperature change. *Sci. Rep.* 7, 1–10. <https://doi.org/10.1038/s41598-017-01451-7>.
- Kobashi, T., Severinghaus, J.P., Brook, E.J., Barnola, J., Grachev, A.M., 2007. Precise timing and characterization of abrupt climate change 8200 years ago from air trapped in polar ice. *Quat. Sci. Rev.* 26, 1212–1222. <https://doi.org/10.1016/j.quascirev.2007.01.009>.
- Kohl, C.P., Nishiizumi, K., 1992. Chemical isolation of quartz for measurement of in-situ-produced cosmogenic nuclides. *Geochem. Cosmochim. Acta* 56, 3583–3587.
- Kuhn, M., 2003. Redistribution of snow and glacier mass balance from a hydro-meteorological model. *J. Hydrol.* 282, 95–103. [https://doi.org/10.1016/S0022-1694\(03\)00256-7](https://doi.org/10.1016/S0022-1694(03)00256-7).
- Lal, D., 1991. Cosmic ray labeling of erosion surfaces: in situ nuclide production rates and erosion models. *Earth Planet Sci. Lett.* 104, 424–439.
- Lamp, J.L., Young, N.E., Koffman, T., Schimmelpfennig, I., Tuna, T., Bard, E., Schaefer, J.M., 2019. Update on the cosmogenic in situ ^{14}C laboratory at the Lamont-Doherty Earth observatory. *Nucl. Instrum. Methods Phys. Res. B* 456, 157–162. <https://doi.org/10.1016/j.nimb.2019.05.064>.
- Lecavalier, B.S., Fisher, D.A., Milne, G.A., Vinther, B.M., Tarasov, L., Huybrechts, P., Lacelle, D., Main, B., Zheng, J., Bourgeois, J., Dyke, A.S., 2017. High Arctic Holocene temperature record from the Agassiz Ice Cap and Greenland Ice Sheet evolution. *Proc. Natl. Acad. Sci. Unit. States Am.* 114, 5952–5957. <https://doi.org/10.1073/pnas.1616287114>.
- LeGrande, A.N., Schmidt, G.A., Shindell, D.T., Field, C.V., Miller, R.L., Koch, D.M., Faluvegi, G., Hoffman, G., 2006. Consistent simulations of multiple proxy responses to an abrupt climate change event. *Proc. Natl. Acad. Sci. Unit. States Am.* 103, 837–842.
- Lenton, T.M., 2011. Early warning of climate tipping points. *Nat. Clim. Change* 1, 201–209. <https://doi.org/10.1038/nclimate1143>.
- Lloyd, J.M., Park, L.A., Kuijpers, A., Moros, M., 2005. Early Holocene palaeoceanography and deglacial chronology of Disko Bugt, west Greenland. *Quat. Sci. Rev.* 24, 1741–1755. <https://doi.org/10.1016/j.quascirev.2004.07.024>.
- Lowell, T.V., 1995. The application of radiocarbon age estimates to the dating of glacial sequences: An example from the Miami sublobe, Ohio, U.S.A. *Quat. Sci. Rev.* 14, 85–99. [https://doi.org/10.1016/0277-3791\(94\)00113-P](https://doi.org/10.1016/0277-3791(94)00113-P).
- MacGregor, K., Anderson, R., Anderson, S., Waddington, E., 2000. Numerical simulations of glacial-valley longitudinal profile evolution. *Geology* 28, 1031–1034.
- Margreth, A., Gosse, J.C., Dyke, A.S., 2017. Wisconsinan and early Holocene glacial dynamics of Cumberland Peninsula, Baffin Island, Arctic Canada. *Quat. Sci. Rev.* 168, 79–100. <https://doi.org/10.1016/j.quascirev.2017.04.033>.
- Margreth, A., Gosse, J.C., Dyke, A.S., 2016. Quantification of subaerial and episodic subglacial erosion rates on high latitude upland plateaus: Cumberland Peninsula, Baffin Island, Arctic Canada. *Quat. Sci. Rev.* 133, 108–129. <https://doi.org/10.1016/j.quascirev.2015.12.017>.
- Marrero, S.M., Phillips, F.M., Borchers, B., Lifton, N., Aumer, R., Balco, G., 2016. Cosmogenic nuclide systematics and the CRONUScal program. *Quat. Geochronol.* 31, 160–187. <https://doi.org/10.1016/j.quageo.2015.09.005>.
- Miller, G.H., 1973. Late Quaternary Glacial and Climatic History of Northern Cumberland Peninsula, Baffin Island, N.W.T., Canada. *Quater. Res.* 3, 561–583.
- Miller, G.H., Dyke, A.S., 1974. Proposed Extent of Late Wisconsin Laurentide Ice on Eastern Baffin Island. *Geology* 2, 125–130.
- Miller, G.H., Lehman, S.J., Refsnider, K.A., Southon, J.R., Zhong, Y., 2013. Unprecedented recent summer warmth in Arctic Canada. *Geophys. Res. Lett.* 40, 5745–5751. <https://doi.org/10.1002/2013GL057188>.
- Miller, G.H., Wolfe, A.P., Steig, E.J., Sauer, P.E., Kaplan, M.R., Briner, J.P., 2002. The Goldilocks dilemma: big ice, little ice, or “just-right” ice in the Eastern Canadian Arctic. *Quat. Sci. Rev.* 21, 33–48. [https://doi.org/10.1016/S0277-3791\(01\)00085-3](https://doi.org/10.1016/S0277-3791(01)00085-3).
- Morrill, C., Ward, E.M., Wagner, A.J., Otto-Bliesner, B.L., Rosenbloom, N., 2014. Large sensitivity to freshwater forcing location in 8.2 ka simulations. *Paleoceanography* 29, 930–945. <https://doi.org/10.1002/2014PA002669>.
- Nichols, K.A., Goehring, B.M., 2019. Isolation of quartz for cosmogenic in situ ^{14}C analysis. *Geochronology* 1, 43–52.
- Nishiizumi, K., Imamura, M., Caffee, M.W., Southon, J.R., Finkel, R.C., McAninch, J., 2007. Absolute calibration of ^{10}Be AMS standards. *Nucl. Instrum. Methods Phys. Res. B* 258, 403–413. <https://doi.org/10.1016/j.nimb.2007.01.297>.
- Osterman, L.E., Nelson, A.R., 1989. Latest Quaternary and Holocene paleoceanography of the eastern Baffin Island continental shelf, Canada: benthic foraminiferal evidence. *Can. J. Earth Sci.* 26, 2236–2248. <https://doi.org/10.1139/e89-190>.
- Paull, T.M., Finkelstein, S.A., Gajewski, K., 2017. Interactions between climate and landscape drive Holocene ecological change in a High Arctic lake on Somerset Island, Nunavut, Canada. *Arctic Sci.* 3, 17–38.

- Pendleton, S.L., Miller, G.H., Lifton, N., Lehman, S.J., Southon, J., Crump, S.E., Anderson, R.S., 2019. Rapidly receding Arctic Canada glaciers revealing landscapes continuously ice-covered for more than 40,000 years. *Nat. Commun.* 10 <https://doi.org/10.1038/s41467-019-08307-w>.
- Perner, K., Moros, M., Jennings, A., Lloyd, J.M., Knudsen, K.L., 2013. Holocene palaeoceanographic evolution off West Greenland. *Holocene* 23, 374–387. <https://doi.org/10.1177/0959683612460785>.
- Putkonen, J., O'Neal, M., 2006. Degradation of unconsolidated Quaternary landforms in the western North America. *Geomorphology* 75, 408–419. <https://doi.org/10.1016/j.geomorph.2005.07.024>.
- Putkonen, J., Swanson, T., 2003. Accuracy of cosmogenic ages for moraines. *Quater. Res.* 59, 255–261. [https://doi.org/10.1016/S0033-5894\(03\)00006-1](https://doi.org/10.1016/S0033-5894(03)00006-1).
- Rahmstorf, S., 2003. Timing of abrupt climate change: A precise clock. *Geophys. Res. Lett.* 30, 21–24. <https://doi.org/10.1029/2003GL017115>.
- Rasmussen, S.O.Å., Vinther, B.M., Clausen, H.B., Andersen, K.K., 2007. Early Holocene climate oscillations recorded in three Greenland ice cores. *Quat. Sci. Rev.* 26, 1907–1914. <https://doi.org/10.1016/j.quascirev.2007.06.015>.
- Reimer, P.J., Bard, E., Bayliss, A., Beck, J.W., Blackwell, P.G., Ramsey, C.B., Buck, C.E., Cheng, H., Edwards, R.L., Friedrich, M., Grootes, P.M., Guilderson, T.P., Hafflidason, H., Hajdas, I., Hatte, C., Heaton, T.J., Hoffmann, D.L., Hogg, A.G., Hughen, K.A., Kaiser, K.F., Kromer, B., Manning, S.W., Niu, M., Reimer, R.W., Richards, D.A., Scott, E.M., Southon, J.R., Staff, R.A., Turney, C.S.M., van der Plicht, J., 2013. IntCal13 and Marine 13 Radiocarbon Age Calibration Curves 0–50,000 Years Cal Bp. *Radiocarbon* 46, 1869–1887. https://doi.org/10.2458/azu_js_rc.46.4183.
- Rinterknecht, V.R., Clark, P.U., Raisbeck, G.M., Yiou, F., Bitinas, A., Brook, E.J., Marks, L., Zelts, V., Lunlka, J.-P., Pavlovskaya, I.E., Piotrowski, J.A., Raukas, A., 2006. The last deglaciation of the southeastern sector of the Scandinavian Ice Sheet. *Science* 311, 1449–1452. <https://doi.org/10.1126/science.1120702>.
- Rood, D.H., Burbank, D.W., Finkel, R.C., 2011. Chronology of glaciations in the Sierra Nevada, California, from ^{10}Be surface exposure dating. *Quat. Sci. Rev.* 30, 646–661. <https://doi.org/10.1016/j.quascirev.2010.12.001>.
- Schaefer, J.M., Denton, G.H., Kaplan, M., Putnam, A., Finkel, R.C., Barrell, D.J.A., Andersen, B.G., Schwartz, R., Mackintosh, A., Chinn, T., Schlüchter, C., 2009. High-frequency Holocene glacier fluctuations in New Zealand differ from the northern signature. *Science* 324, 622–625. <https://doi.org/10.1126/science.1169312>.
- Schulz, M., 2002. On the 1470-year pacing of Dansgaard-Oeschger warm events. *Paleogeography* 17.
- Sgubin, G., Swingedouw, D., Drijfhout, S., Mary, Y., Bennabi, A., 2017. Abrupt cooling over the North Atlantic in modern climate models. *Nat. Commun.* 8, 1–12. <https://doi.org/10.1038/ncomms14375>.
- Sheldon, C., Jennings, A., Andrews, J.T., Ó Cofaigh, C., Hogan, K., Dowdeswell, J.A., Seidenkrantz, M.S., 2016. Ice stream retreat following the LGM and onset of the west Greenland current in Uummannaq Trough, west Greenland. *Quat. Sci. Rev.* 147, 27–46. <https://doi.org/10.1016/j.quascirev.2016.01.019>.
- Stone, J.O., 2000. Air pressure and cosmogenic isotope production. *J. Geophys. Res.* 105, 23753–23759.
- Stuiver, M., Reimer, P., Reimer, R., 2018. CALIB 7.1 [WWW program] at. <http://calib.org>.
- Tang, C.C.L., Ross, C.K., Yao, T., Petrie, B., DeTracey, B.M., Dunlap, E., 2004. The circulation, water masses and sea-ice of Baffin Bay. *Prog. Oceanogr.* 63, 183–228. <https://doi.org/10.1016/j.pcean.2004.09.005>.
- Thomas, E.R., Wolff, E.W., Mulvaney, R., Steffensen, J.P., Johnsen, J., Arrowsmith, C., White, J.W.C., Vaughn, B., Popp, T., 2007. The 8.2 ka event from Greenland ice cores. *Quat. Sci. Rev.* 26, 70–81. <https://doi.org/10.1016/j.quascirev.2006.07.017>.
- von Blanckenburg, F., Belshaw, N.S., O'Nions, R.K., 1996. Separation of ^9Be and cosmogenic ^{10}Be from environmental materials and SIMS isotope dilution analysis. *Chem. Geol.* 129, 93–99. [https://doi.org/10.1016/0009-2541\(95\)00157-3](https://doi.org/10.1016/0009-2541(95)00157-3).
- Wanner, H., Solomina, O., Grosjean, M., Ritz, S.P., Jetel, M., 2011. Structure and origin of Holocene cold events. *Quat. Sci. Rev.* 30, 3109–3123. <https://doi.org/10.1016/j.quascirev.2011.07.010>.
- Weidick, A., 1972. Holocene shorelines and glacial stages in Greenland—an attempt at correlation. *Rapp. - Grn. Geol. Undersøgelse* 41, 1–39.
- Weidick, A., 1968. Observations on some Holocene glacier fluctuations in West Greenland. *Meddelelser om Grønland* 165, 1–202.
- Young, N.E., Briner, J.P., Maurer, J., Schaefer, J.M., 2016. ^{10}Be measurements in bedrock constrain erosion beneath the Greenland Ice Sheet margin. *Geophys. Res. Lett.* 43, 1–12. <https://doi.org/10.1002/2016GL070258>.
- Young, N.E., Briner, J.P., Miller, G.H., Lesnek, A.J., Crump, S.E., Thomas, E.K., Pendleton, S.L., Cuzzone, J., Lamp, J., Zimmerman, S., Caffee, M., Schaefer, J.M., 2020a. Deglaciation of the Greenland and Laurentide ice sheets interrupted by glacier advance during abrupt coolings. *Quat. Sci. Rev.* 229 <https://doi.org/10.1016/j.quascirev.2019.106091>.
- Young, N.E., Briner, J.P., Rood, D.H., Finkel, R.C., 2012. Glacier extent during the Younger Dryas and 8.2-ka event on Baffin Island, Arctic Canada. *Science* 337, 1330–1333. <https://doi.org/10.1126/science.1222759>.
- Young, N.E., Briner, J.P., Rood, D.H., Finkel, R.C., Corbett, L.B., Bierman, P.R., 2013a. Age of the Fjord Stade moraines in the Disko Bugt region, western Greenland, and the 9.3 and 8.2 ka cooling events. *Quat. Sci. Rev.* 60, 76–90. <https://doi.org/10.1016/j.quascirev.2012.09.028>.
- Young, N.E., Briner, J.P., Schaefer, J.M., Miller, G.H., Lesnek, A.J., Crump, S.E., Thomas, E.K., Pendleton, S.L., Cuzzone, J., Lamp, J., Zimmerman, S., Caffee, M., 2020b. Reply to Carlson (2020) comment on “Deglaciation of the Greenland and Laurentide ice sheets interrupted by glacier advance during abrupt coolings. *Quat. Sci. Rev.* <https://doi.org/10.1016/j.quascirev.2020.106329>.
- Young, N.E., Briner, J.P., Stewart, H.A.M., Axford, Y., Csatho, B., Rood, D.H., Finkel, R.C., 2011. Response of Jakobshavn Isbræ, Greenland, to Holocene climate change. *Geology* 39, 131–134. <https://doi.org/10.1130/G31399.1>.
- Young, N.E., Lamp, J., Koffman, T., Briner, J.P., Schaefer, J., Gjermundsen, E.F., Linge, H., Zimmerman, S., Guilderson, T.P., Fabel, D., Holmes, A., 2018. Deglaciation of coastal south-western Spitsbergen dated with in situ cosmogenic ^{10}Be and ^{14}C measurements. *J. Quat. Sci.* 33, 763–776. <https://doi.org/10.1002/jqs.3058>.
- Young, N.E., Schaefer, J.M., Briner, J.P., Goehring, B.M., 2013b. A ^{10}Be production-rate calibration for the Arctic. *J. Quat. Sci.* 28, 515–526. <https://doi.org/10.1002/jqs.2642>.
- Young, N.E., Schaefer, J.M., Goehring, B., Lifton, N., Schimmelpfennig, I., Briner, J.P., 2014. West Greenland and global in situ ^{14}C production-rate calibrations. *J. Quat. Sci.* 29, 401–406. <https://doi.org/10.1002/jqs.2717>.